



Lava-ice interactions during historical eruptions of Veniaminof Volcano, Alaska and the potential for meltwater floods and lahars

Christopher F. Waythomas¹ · Benjamin R. Edwards² · Thomas P. Miller¹ · Robert G. McGimsey¹

Received: 16 November 2021 / Accepted: 25 July 2022

This is a U.S. Government work and not under copyright protection in the US; foreign copyright protection may apply 2022

Abstract

Veniaminof Volcano on the Alaska Peninsula of southwest Alaska is one of a small group of ice-clad volcanoes globally that erupts lava flows in the presence of glacier ice. Here, we describe the nature of lava-ice-snow interactions that have occurred during historical eruptions of the volcano since 1944. Lava flows with total volumes on the order of 0.006 km^3 have been erupted in 1983–1984, 1993–1994, 2013, and 2018. Smaller amounts of lava ($1 \times 10^{-4} \text{ km}^3$ or less) were generated during eruptions in 1944 and 2021. All known historical eruptions have occurred at a 300-m-high cinder cone (informally named cone A) within the 8×10 -km-diameter ice-filled caldera that characterizes Veniaminof Volcano. Supraglacial lava flows erupted at cone A, resulted in minor amounts of melting and did not lead to any significant outflows of water in nearby drainages. Subglacial effusion of lava in 1983–1984, 2021 and possibly in 1944 and 1993–1994 resulted in more significant melting including a partially water-filled melt pit, about 0.8 km^2 in area, that developed during the 1983–1984 eruption. The 1983–1984 event created an impression that meltwater floods from Mount Veniaminof's ice-filled caldera could be significant and hazardous given the large amount of glacier ice resident within the caldera (ice volume about 8 km^3). To date, no evidence supporting catastrophic outflow of meltwater from lava-ice interactions at cone A has been found. Analysis of imagery from the 1983–1984 eruption shows that the initial phase erupted englacial lavas that melted ice/snow/firn from below, producing surface subsidence outward from the cone with no discernable surface connection to the summit vent on cone A. This also happened during the 2021 eruption, and possibly during the 1993–1994 eruption although meltwater lakes did not form during these events. Thus, historical eruptions at Veniaminof Volcano appear to have two different modes of effusive eruptive behavior, where lava reaches the ice subglacially from flank vents, or where lava flows are erupted subaerially from vents near the summit of cone A and flow down the cone on to the ice surface. When placed in the context of global lava-ice eruptions, in cases where lava flows melt the ice from the surface downward, the main hazards are from localized phreatic explosions as opposed to potential flood/lahar hazards. However, when lava

Extended author information available on the last page of the article

effusion/emplacement occurs beneath the ice surface, melting is more rapid and can produce lakes whose drainage could plausibly produce localized floods and lahars.

Keywords Veniaminof Volcano · Lava flows · Ice melt · Hazards · Historical eruptions

1 Introduction

In this paper, we report on lava flow interaction with ice and snow during historical eruptions of Veniaminof Volcano, Alaska (Fig. 1). Effusive, lava-producing eruptions at snow and ice-clad stratovolcanoes are less common than explosive events (Major and Newhall 1989; Edwards et al. 2012, 2015; Oddsson et al. 2016; Smellie and Edwards 2016). When

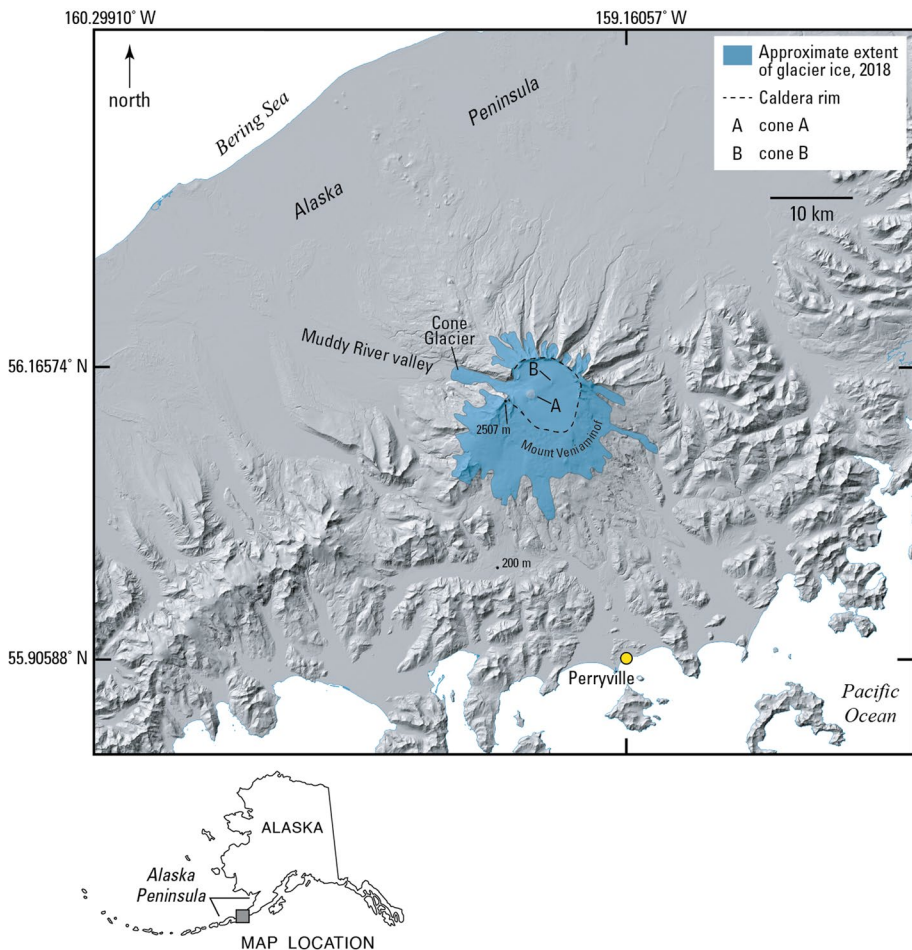


Fig. 1 Location of Veniaminof Volcano on the Alaska Peninsula of southwestern Alaska. Blue area shows the extent of glacier ice on the volcano as of September 2018. The ice cover was mapped on a Sentinel-2 satellite image (spatial resolution 15 m), acquired on September 11, 2018. Shaded relief base from USGS IfSar digital elevation data, 5 m resolution

they occur, they provide opportunities to investigate how lava flows interact with snow and ice. These interactions typically produce meltwater, and it is important to determine the rate of meltwater formation and the volume of water produced to better address flood and lahar hazards at snow and ice clad volcanoes (Delgado Granados et al. 2015), as well as for obtaining a better understanding of the role of external water in eruption dynamics. Magma-water interaction processes that occur near the Earth's surface are known either as hydrovolcanism (Sheridan and Wohletz 1983; Wohletz et al. 2013), if the water source is groundwater, lakes or oceans, or glaciovolcanism if the source of water is melting ice (Smellie and Edwards 2016). Eruptions that involve external water can be highly explosive (Wohletz 1986; Valentine et al. 2014) and can facilitate the production of fine ash (Self and Sparks 1978; Heiken and Wohletz 1985), ash aggregates (Van Eaton et al. 2012), the occurrence of high-amplitude volcanic tremor (Haney 2014), and the generation of pyroclastic flows (Belousov et al. 2011).

External water derived primarily from the melting of snow and ice plays a key role in many global eruptions (Barr et al. 2018; Edwards et al. 2020), but because of the remote location of snow and ice clad volcanoes in Alaska, observation and study of glaciovolcanic processes there is limited. Over time, observations spanning multiple eruptions are useful for describing the nature of the interaction of hot eruptive products with ice and snow and the resulting effects, hazards, and impacts (Waythomas 2014; Smellie and Edwards 2016). In this context, we provide the first synthesis of historical lava-ice interactions at Veniaminof Volcano, a large, glaciated stratovolcano on the Alaska Peninsula of southwest Alaska (Fig. 1). We review and evaluate the evidence for lava-ice interaction during historical eruptions since 1944, document the extent of ice and snow melt, and address the potential for meltwater generation and ensuing flood and lahar events triggered by eruptions of the historically active intracaldera cone. Many volcanoes in Alaska support significant quantities of ice and snow, commonly $> 1 \text{ km}^3$ in volume (Waythomas 2014). Thus, the potential for melting snow and ice during eruptive activity throughout the Aleutian arc has important implications for lahar development and associated hazards. Although few of the drainages potentially impacted are inhabited or contain significant infrastructure, these areas include important biological resources and habitat that could be adversely affected by volcanic mass flows (Schaefer et al. 2008).

The 1983–1984 eruption of Veniaminof resulted in the formation of 0.8 km^2 melt pit in the glacier ice surrounding the historically active vent. The ephemeral lake that formed in the melt pit raised numerous questions about the potential for catastrophic drainage from such lakes and associated lahar and flood hazards in the drainages extending from the volcano. This study will address this hazard and provide an analysis of meltwater generation by lava flows and the likelihood for hazardous meltwater-derived floods and lahars during future eruptions.

2 Geologic setting

Veniaminof Volcano is a dacite to basalt stratovolcano about 350 km^3 in volume, located on the Alaska Peninsula (56.198 N , $- 159.393 \text{ W}$) about 35 km north of the village of Perryville and roughly midway between the Bering Sea and the North Pacific Ocean (Fig. 1). The volcano is characterized by a circular 8 by 10 km diameter ice-filled summit caldera (Fig. 2; highest point on the caldera rim is 2507 m above sea level) that formed during significant eruptions in late Pleistocene–Holocene time (Miller et al.



Fig. 2 View of the caldera icefield at Veniaminof Volcano showing intracaldera cones A and B and ice marginal cinder cones labeled C. View is toward the northwest. The distance from cone A to cone B is about 3 km. Note minor ash and vapor emissions at cone A. Photograph by Zachary Finley, September 14, 2018

2002). Veniaminof was extensively glaciated during the late Quaternary (Detterman et al. 1981). The flanks of the volcano have been deeply incised by glacier erosion and numerous glaciated valleys with nearly vertical valley walls are characteristic, except on parts of the south flank where a broad lobe of ice drapes over a morphologically subdued caldera rim.

Veniaminof Volcano is one of the largest and most active volcanoes in the Aleutian arc and has erupted at least 19 times since 1830–1840 (Table 1; Miller et al. 1998; <https://www.avo.alaska.edu>, 2002). All known historical eruptions have occurred from vents located on a 300 m high, intracaldera cinder cone about 1 km in diameter, and roughly 1.2 km² in area (cone A, Fig. 1). The volume of the cone is about 0.1 km³. Historical eruptions have been characterized by small-to-moderate Strombolian explosions (generally VEI 1–3) interspersed with episodes of lava fountaining, low-level emissions of ash and gas, and occasional effusion of small lava flows (Miller et al. 1998; Smellie and Edwards 2016; Waythomas 2021). Ash plumes associated with historical eruptions have been relatively small and usually do not reach more than about 4–6 km above sea level. Occasional stronger bursts of activity have generated higher rising plumes, such as during the 1939 and 1956 eruptions when ash plumes rose to an estimated 6.1 km above sea level (Miller et al. 1998), and during the 1983–84 eruption when the largest ash plume reached a height of 8 km above sea level (Yount et al. 1985). During the 2018 eruption, an ash cloud reach a height of about 4.5 km above sea level on November 21, 2018 (Loewen et al. 2021; Waythomas et al. 2022).

The caldera icefield has a level flat surface that is interrupted by cone A and a second constructional cone (cone B), but only cone A has significant relief above the ice and snow surface and because of elevated heat flow, is typically snow-free year-round (Fig. 2). Rock and pyroclastic debris on cone B is exposed during times of low snow cover and the cone is clearly a positive topographic feature within the caldera icefield. The eruptive history

Table 1 Historical eruptions of Veniaminof volcano. U=unknown. Volcano Explosivity Index (VEI) values are estimates of the largest event within an eruptive period; in many cases not confirmed with known eruptive volumes

Date	Duration	Maximum ash cloud height (m)	VEI	Comments
1830–1840	U	U	2?	“Flames” and ash emissions observed sometime during nine–ten-year period
1852	U	U	U	Ash emissions
1892	3 days	3200	3?	Explosions, roaring sounds, lava fountaining, ash emission
Nov. 1939	U	U	2?	Ash emission
May–June, 1939	28 days	6100	3?	Explosions, ash emission, lava fountaining
1944	Weeks	U	2?	Ash emissions, flank vent lava flows, see Fig. 2a
1956	~3 months	6100	3?	Ash emissions
1983–1984	~10 months	7800	3	Ash emissions, flank vent lava flows, lava fountaining
1984	~10 days	5400	2?	Explosions, ash emissions in bursts
1993–1994	~13 months	5500	2	Ash emissions, flank vent lava flows
1995	~7 months	U	1–2?	Explosions, possible flank lava flows
2002–2003	~5 months	<1000	1	Minor steam and ash bursts, explosions, ash emissions
2004	~7 months	3500	2	Steam and ash bursts
2005	~1.5 months	4000	2	Minor lava fountaining, steam and ash bursts
2005	~3 months	3000	1	Minor ash emissions, ash and steam bursts
2006	~8 months	2300	1	Intermittent steam and ash bursts
2013	~4 months	6100	2–3	Ash emissions, flank lava flows, lava fountaining
2018	~4 months	4900	2	Ash emissions, flank lava flows, lavafountaining
2021	~1 month	3000	0–1	Ash emissions, subglacial lava effusion

of cone B is unknown, and one lava sample collected in 1973 was basaltic in composition (53.1 wt.% SiO₂, Yount et al. 1985). Cone A is composed of rubbly ‘a’ lava flows interbedded with near vent spatter, bombs, lapilli and ash. Two lava samples collected from cone A in 1973 and 1974 contained 53.8 and 55.4 wt.% SiO₂ (T.P. Miller USGS unpublished data). The lava flows erupted in 2018 were basaltic andesite in composition (54 ± 0.7 wt.% SiO₂; Loewen et al. 2021).

At least three additional 300–400 m diameter cinder cones extend above the ice surface along the southern margin of the caldera icefield (Fig. 2). These cones are fresh-appearing and do not appear obviously glaciated. It is possible that one or more of them were active historically, but their eruptive history is unknown.

Holocene pyroclastic flow, lahar, and tephra deposits mantle the distal flanks of the volcano and record multiple caldera-forming eruptions and several smaller explosive events (Miller and Smith 1987; Miller et al. 2002; Waythomas et al. 2015). The pre-Holocene eruptive history of the volcano is constrained by ⁴⁰Ar/³⁹Ar and K–Ar dating of basalt, andesite, and dacite lavas and indicates a ca. 340 ka long record of eruptive activity punctuated by caldera-forming eruptions of the late Quaternary (Calvert et al. 2021; Calvert et al. 2005; Bacon et al. 2003).

The area of glacier ice on Veniaminof as depicted on U.S. Geological Survey topographic maps surveyed in 1963 and based on aerial photographs taken in 1957 and 1962 was about 340 km². Glacier outlines and areas in the Global Land Ice Measurements from Space (GLIMS) database indicate a total ice area of 286 km² as of 2010 (Raup et al. 2007, RGI Consortium 2012). The ice extent determined from a Sentinel-2 satellite image acquired on September 11, 2018, near the end of the melt season was about 290 km². The estimated ice volume covering the volcano using an average ice thickness of 50 m is about 14.5 km³ and more than half of this amount (8 km³) resides within the caldera (Welch et al. 2007). Ice on the south flank of the edifice forms a broad ice apron with several outlet glaciers (Fig. 1). Glaciers on the north, east and west sides of the caldera icefield occupy breaches in the caldera rim (Fig. 1).

Glacier equilibrium line altitudes of the main outlet glaciers are about 1500–1700 m, roughly 200–400 m below the surface of the icefield and thus all the caldera icefield is within the accumulation zone. The surface topography of the outlet glaciers shows no unusual crevasse or moraine patterns indicative of fast flow or surging behavior.

An ice-radar survey of the caldera icefield was completed in July 2005 (Welch et al. 2007). The purpose of the survey was to determine ice thickness, better define the southern rim of the caldera, and to identify potential subglacial pathways for meltwater. Although the distribution of crevasses and soft snow conditions prohibited survey of the entire caldera icefield, roughly two thirds of the icefield was surveyed. The surface altitude of the icefield in July 2005 was about 1900 m and the topography of the surface was nearly flat (< 1°). Ice as thick as 475 m is present in the southern part of the caldera (Fig. 3). Evidence of ponded subglacial water was not apparent in the sounding data, and it is possible that parts of the caldera icefield are frozen to the bed (Welch et al. 2007).

3 Methods

While most of this paper describes visual observations of Mount Veniaminof eruptions, we have also quantified lava aerial extents using aerial photography, interferometric synthetic aperture radar (IfSAR; <http://agc.dnr.alaska.gov/elevation.html>), Sentinel-2, WorldView and Landsat scenes. Measurements were made using QGIS 3.14. Estimates of ice cauldron depths are from the IfSAR Digital Terrain Model (DTM; US Geological Survey 2018) acquired June 16–July 3, 2018, as well as from aerial photographs obtained on August 26, 1983, using Agisoft Metashape Pro 1.6.4 (build 10,928). Additional digital elevation data and photographs were acquired during aerial overflights of the caldera in 2018 and 2019 (Dieterich et al. 2021).

The data obtained in 2018 and 2019 were used to produce a structure-from-motion (SfM) digital elevation model (Dieterich et al. 2021). Vertical aerial photographs were processed with Agisoft Metashape using SfM methods and a high-resolution orthophoto (0.3 m cell size) and DTM (0.58 m cell size). The root-mean-square error of the DTM is 2.3 m, estimated from control points on the USGS 2018 IfSAR DTM.

It was not possible to determine the thickness of historically emplaced lava flows at cone A, except for the 2018 lavas where DEM's were used to estimate flow thickness (Loewen et al. 2021). Observations and photographs of historical lava flows indicate that all flows are at least 1 m thick but likely thicker along flow margins, in levees, and where flows overran previously emplaced flows. To date, the DEM-based analysis of lava flow thickness by Loewen et al. (2021) is the best estimate of lava thickness variation for the types of lavas

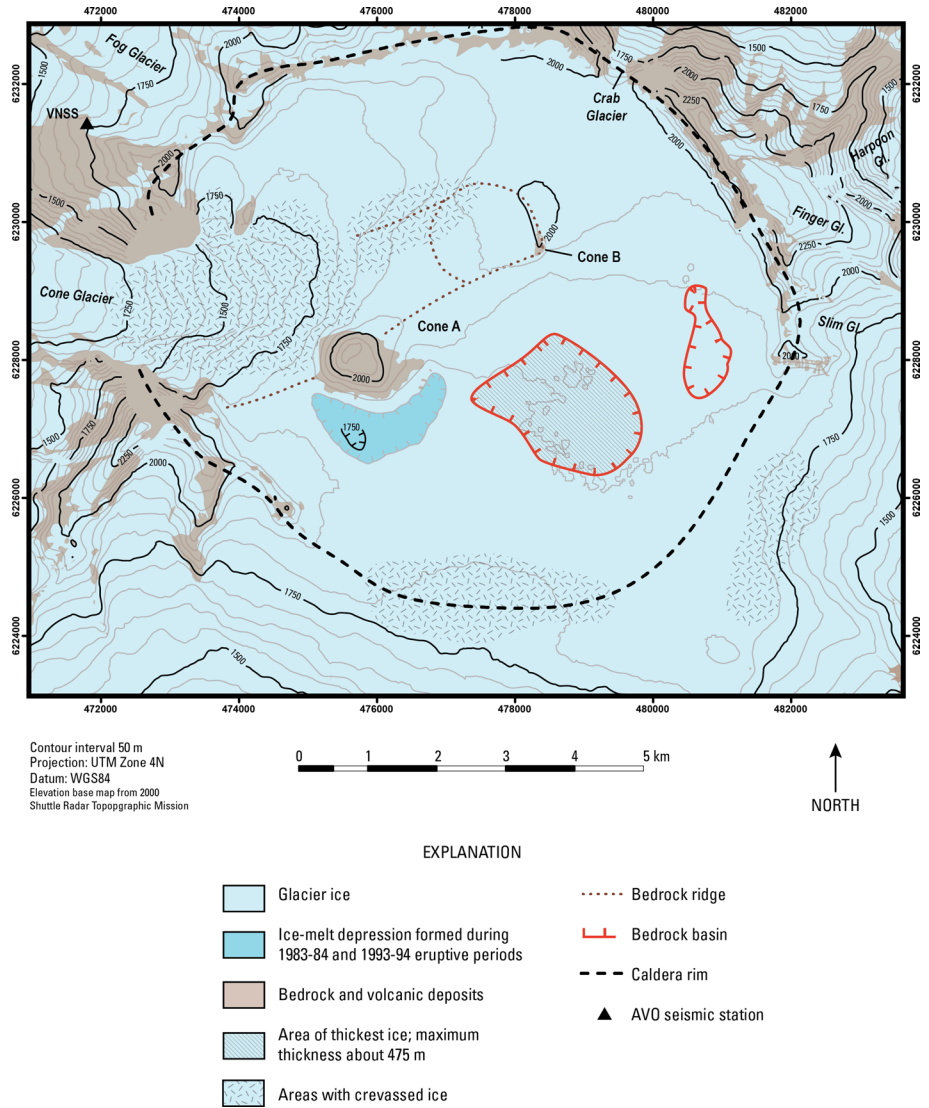


Fig. 3 Topography and features of the Veniaminof ice-filled caldera based on an ice-radar survey completed in 2005 (modified from Welch et al. 2007)

emplaced at cone A, given the similarity in eruptive style of the events described here. The 2018 lava flows ranged in thickness from <3 m to as much as 15 m with an overall average thickness of about 9 m +/- 50% (Loewen et al. 2021). As we will show, the average thickness value used affects the volume calculations if a simple area-thickness calculation is made but does not appreciably affect ice melt rates based on lava flow thickness (Wilson and Head 2007).

Hypothetical lahars originating from a meltwater lake in the caldera were evaluated using LaharZ, a GIS-based lahar inundation mapping tool that portrays the areas likely to be inundated by lahars of known or reasonably estimated initial volumes (Iverson et al. 1998; Schilling 2014). LaharZ is implemented in ArcGis Pro and utilizes a digital-elevation model of the areas of interest. We used the US Geological Survey 1 arc-second, 1 × 1 degree DEM's of the Veniaminof area (approximately 30 m resolution) and converted them to ESRI grid format for use in LaharZ. Additional information about the application of LaharZ is given in Sect. 7.

4 Lava-ice interactions during historical eruptions

The following section of the paper presents observations of cone A lava flows that developed during historical eruptions since 1944. Because Cone A is surrounded by glacier ice and snow, effusive eruptions from the cone will most likely produce lava-ice interactions. However, even though as many as 20 periods of eruptive activity from the cone are documented, lava-ice interaction has been observed for only six of those events (1944, 1983–1984, 1993–1994, 2013, 2018, 2021). Steam plumes have been noted during several other of the 20 eruptive episodes and are commonly a result of lava-ice-snow interaction. This suggests that there may have been other eruptions older than 1944 where lava flows interacted with ice and snow.

4.1 1944 eruption

The earliest historical evidence for lava flows from cone A reaching the icefield within Veniaminof caldera comes from a 1944 oblique aerial photograph that shows an ash plume rising from cone A and a small steam plume just above what appears to be a small melt pit on the ice surface on the southwest side of the cone (Fig. 4a). It is unclear from this photograph if the lava flow was initially emplaced subglacially or from a vent higher up on cone A. A second photograph shows cone A in eruption and what appears to be a circular melt pit containing a meltwater lake on the southwest side of the cone (Fig. 4b). The photograph was taken between 1942–1944 with 1944 being the most likely eruption date. No lava flows extending from the summit crater of cone A are apparent in the photograph which implies an eruption from a (subglacial?) flank vent near the base of cone A was responsible for producing the melt pit.

4.2 1983–1984 eruption

The 1983–1984 eruption of Veniaminof Volcano lasted from early June 1983 to about mid-April 1984 (Yount et al. 1985). Information about the 1983–1984 eruption came from

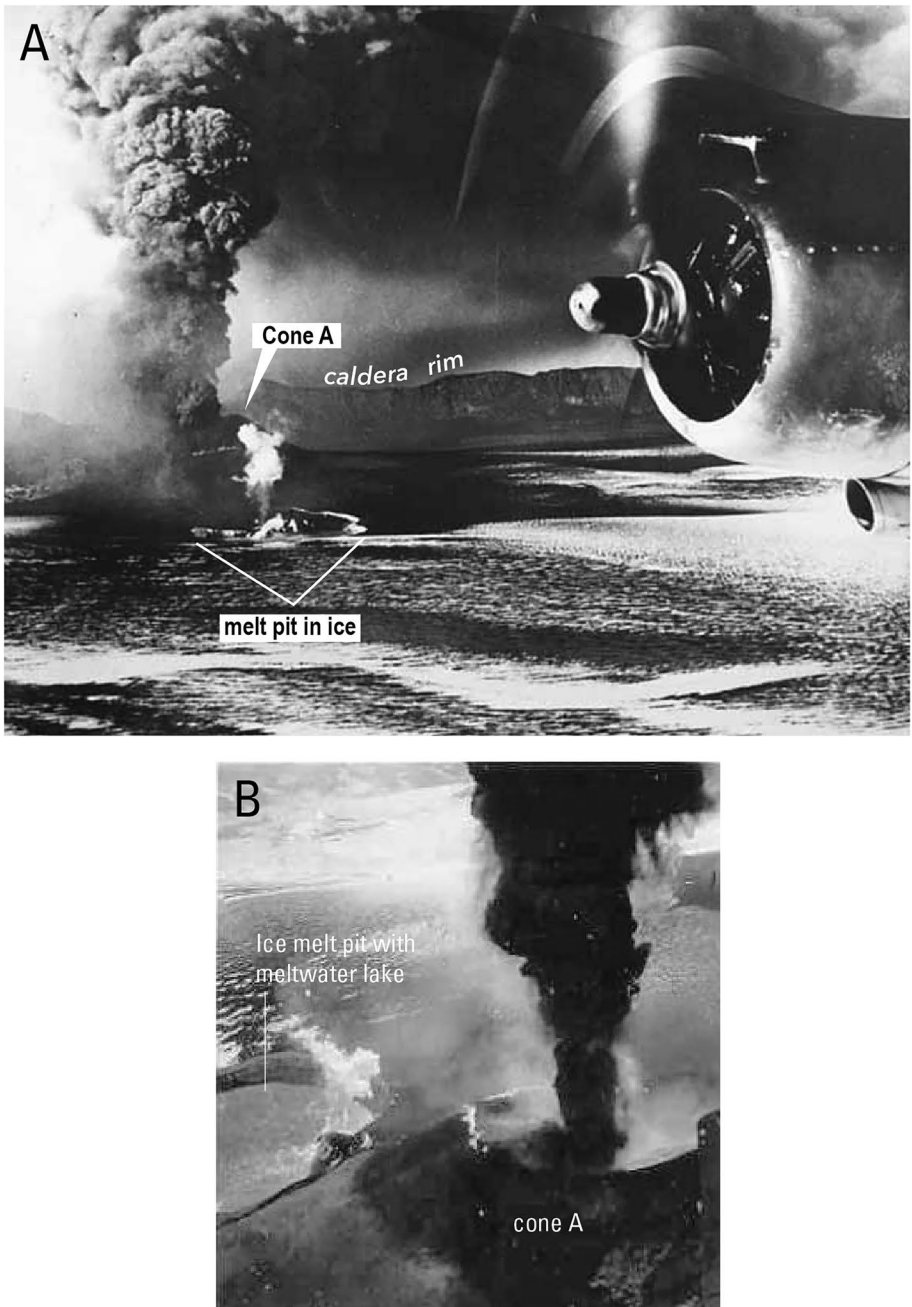


Fig. 4 Photographs of the 1944 eruption of cone A. **A** Cone A in eruption, March 30, 1944. The photo also shows a melt pit at the base of cone A likely generated by a lava flow. Scale of the photograph is not known but the relief of cone A above the caldera icefield is about 300m. View is toward the east. Photograph courtesy of the San Francisco Call-Bulletin, Aleutian Islands Photographs, 1942–1948 Collection. **B** Cone A, ice melt pit, and meltwater lake, view is toward the south—southwest. Date of photograph not known, but likely 1944. Image courtesy of Lawrence Tyree

observations made during aerial overflights of the volcano in June, July, and October 1983, and January 1984 (Yount et al. 1985). The photographs and observations made during these overflights are the basis for the interpretations that follow regarding the nature of lava-ice interactions during this eruptive period. Additional information about the eruption can be found in Yount et al. (1985) and on the Alaska Volcano Observatory web site (<https://www.avo.alaska.edu/volcanoes/activity.php?volcname=Veniaminof&page=basic&eruptionid=319>).

Observations made in early June 1983 found an ongoing eruption at cone A, characterized by low-level lava fountaining and Strombolian bursts, which produced concentrated, dark ash clouds (Yount et al. 1985). Aerial observations made on June 7, 1983, indicated that an approximately 90-m-wide 300-m-long linear subsidence depression and a 400-m-diameter, 20–30-m-deep, circular, ice cauldron-like depression in the caldera ice-field immediately south of cone A had formed (Fig. 5a). These features record effusion of a subglacial lava flow (LF1 on Fig. 5a) from a subglacial vent on the southwest flank of cone A (Yount et al. 1985). By June 9, 1983, a second vent was also effusing lava, but the flow (LF2 on Fig. 5b) was entirely supraglacial and extended out over the ash covered ice at the base of cone A. Observations made on June 15, 1983, indicated a second subglacial lava flow (LF3 on Fig. 5c) was emplaced just south of the initial subglacial flow, and it also produced a small ice cauldron.

The combined thermal effects of the subglacial lava flows emplaced earlier, and the supraglacial lava flow evident on June 9, led to the formation of a 1200-m-long, 200–500-m-wide, 50–100-m-deep, vertical-walled melt pit in the glacier ice on the southwest side of cone A. As of July 26, 1983 the pit had an area of about 0.8 km² (Fig. 6). The melt pit contained an ephemeral lake whose depth was unknown but probably on the order of 10–30 m based on reported heights of the melt pit wall (Yount et al. 1985). Continued lava effusion from cone A led to the formation of a southward-building lava delta (Fig. 6; Yount et al. 1985). A semicircular ice cavity was observed in the ice wall at the east end of the lake (Fig. 7). Initially, this feature was interpreted as a subglacial meltwater tunnel but is more likely a melt cavity produced by a subglacial or englacial lava flow. While no evidence indicates that the meltwater lake was ever deep enough (i.e., water depth > 0.9 × ice thickness) to develop the hydraulic head required to permit subglacial water flow, it is possible that the cavity developed within more porous firn at the firn–ice transition (typically 40–80 m depth; Cuffy and Paterson 2010), which would imply englacial rather than subglacial lava effusion.

It is clear from aerial observations that the 1983–1984 eruption began subglacially and resulted in the formation of circular ice depressions, or ice cauldrons, similar to those observed in Iceland during eruptions at Grimsvötn (Björnsson 2003) and at Gigjökull (Oddsson et al. 2016) only smaller. Eventually the ice cauldrons collapsed, coalesced, and formed an elongate melt pit that contained a meltwater lake that as of August 26, 1983, had an area of about 0.4 km² (Fig. 8a). For lake depths of 10–30 m, the meltwater lake volume would be 4–12 × 10⁻³ km³. The lava flows in the August 26 aerial photo have an area of about 0.5 km².

4.3 1993–1994 eruption

Eruptive activity at Veniaminof Volcano in 1993 was first observed by passing pilots who reported steam plumes rising from cone A in February 1993 (Neal et al. 1995). Ash

emissions were observed for the first time on July 30, 1993, and thereafter intermittently through August 12, 1993 (Neal et al. 1996). Residents of Perryville observed bursts of incandescent material rising approximately 300 m above the summit on October 7 confirming that an active eruption was in progress (Neal et al. 1996).

Observations made on a U.S. Coast Guard overflight on November 6, 1993, documented the presence of a lava flow on the lower east flank of cone A. The lava flow was contained within a depression in the ice visually estimated to be about 2.0 km long by 0.75 km wide (Fig. 8b; McGimsey et al. 1995). Steam emissions were observed along the margins of the lava flow where it was in contact with glacier ice.

Low-level eruptive activity continued intermittently through the winter of 1993–1994 and occasional minor ash and steam emissions were observed from Perryville (Neal et al. 1995, 1996). Lava effusion was observed on May 9, 1994, during an overflight of the volcano by the Alaska Volcano Observatory (AVO) and the lava flow observed in 1993 remained contained within the oval-shaped melt depression in the ice and snow on the southeast flank of cone A (Fig. 9). A Landsat 5 satellite image obtained on September 26, 1995, shows the approximate extent of subaerial lava emplaced during the 1993–1994 eruptive episode (Fig. 8b). The lava covers an area of about 0.9 km².

Photographs of the 1993–1994 eruption indicate that lava likely erupted from a spatter or cinder cone that developed on the lower east flank of cone A (Fig. 9b). It is not known if the lava was initially erupted subglacially but there likely was a subglacial vent that eventually breached the ice and produced the spatter/cinder cone observed in May 1994 (Fig. 9). There were no observations of any lava flows extending from the summit of cone A to the surrounding glacier ice. Standing water was not evident within the melt pit observed on May 9, 1994. Low-level activity continued intermittently throughout the summer and fall of 1994 (Neal et al. 1995), and elevated surface temperatures associated with cooling lava were detected in satellite data into early 1995 (Neal et al. 1996).

4.4 2013 eruption

The 2013 eruption of Veniaminof Volcano was described in detail by Dixon et al. (2015) and is only summarized below. It began on about June 13 after a seven-day period of gradually increasing levels of seismic tremor and ended by about October 17 (Dixon et al. 2015, Fig. 25). The initial pulse of eruptive activity consisted primarily of minor ash emissions followed by satellite detection of elevated surface temperatures at cone A. From June 13–July 19, at least three lava flows were erupted on the southwest flank of cone A (Fig. 10, lava flows 1, 2, 3). These flows extended a short distance beyond the base of the cone and began to slowly melt into the underlying snow and ice (Fig. 11a). After July 19, the source vent for the lava flows shifted to the east, and lava flows developed on the east flank of cone A (Fig. 10, lava flows 4, 5). The flows on the east side of cone A also extended a short distance beyond the base of the exposed cone and began slowly melting into the underlying snow and ice (Fig. 11b). Elevated surface temperatures were observed in satellite data from June 13–September 20, consistent with reports and observations of lava effusion at cone A (Dixon et al. 2015).

Between September 20 and October 6, seismicity, ash emission, and lava effusion declined appreciably. There was a brief period of lava effusion, explosions, and ash emission from October 6 to 17, but after that, the level of unrest declined gradually, and the eruption ended.

Fig. 5 June 1983 photographs of cone A and lava-ice interaction features. **A** Evidence for subglacial lava flow during the early part of the 1983–84 eruption, June 7, 1983. This is lava flow LF1 in subsequent photographs. View is toward the east. **B** Continued effusion of lava results in a second lava flow (LF2) emplaced subaerially, June 7, 1983. View is toward the east. **C** Evidence for a third lava flow (LF3) that was also emplaced subglacially, June 15, 1983. All photographs by E. Yount, USGS

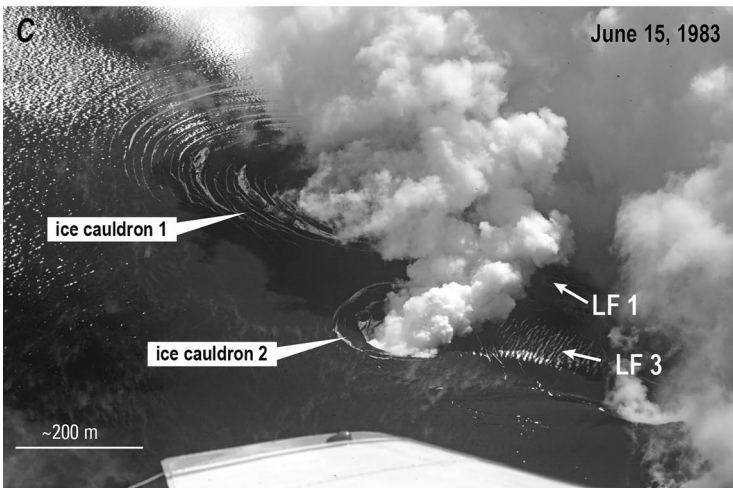
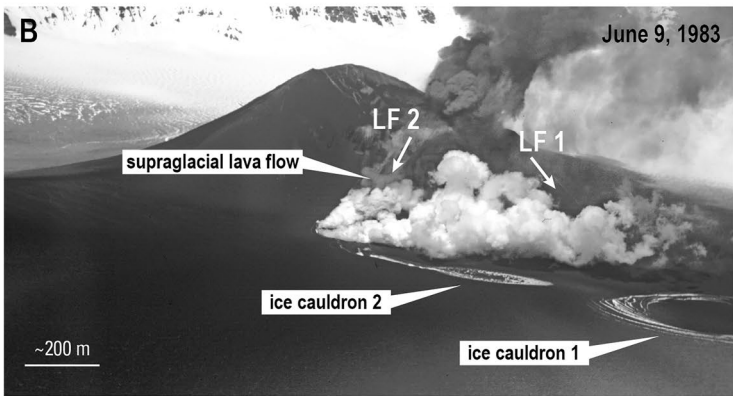
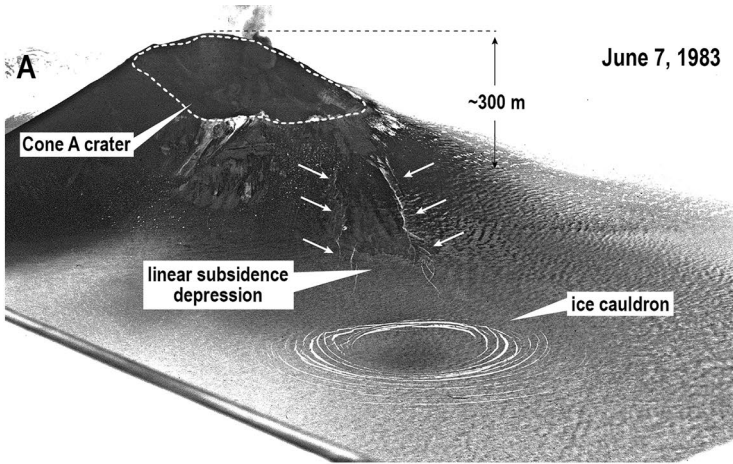
The lava flows emplaced during the 2013 eruption consisted of relatively short, rubbly ‘a’ā flows, approximately 250–1000 m long and 200–250 m wide that extended down the flanks of cone A onto snow and ice at the base of the cone (Fig. 10). There were three general phases of lava effusion beginning with the development of a lava fan on the southwest flank of cone A, effusion of lava on the northeast flank of cone A from two boccos (Fig. 11b), and effusion of lava from vents on the south flank (Fig. 11c).

Due to the eruptive state of the volcano, we were unable to sample the lavas or obtain close-in measurements of lava thickness during visits to the area in July and August. Thermal data on lava flows 4 and 5 were obtained on August 18, 2013, using a handheld Forward Looking Infrared (FLIR) camera. A spot temperature measured on one of the lava flows was 619 °C (Fig. 11d). The total area of lava erupted during the 2013 eruption is about 0.5 km². The thickness of the lava flows is not known, but in context with the 2018 lava flows (Loewen et al. 2021) volumes could be on the order of $4.5 \times 10^{-3} \text{ km}^3 \pm 50\%$.

Observations made throughout the 2013 eruptive period indicated that the melt rates of ice beneath and along margins of the lava flows were relatively slow and did not result in the production of significant volumes of water. No areas of standing water were observed in any of the melt pits, although we did observe robust steaming around the margins of some of the flows where the lavas were close to or in direct contact with glacier ice. The meltwater that was generated may have seeped back into the edifice, gradually flowed away from the eruption site ahead of the lava flows, or ponded somewhere below the glacier surface in the vicinity of the intra-caldera cone and probably refroze. Areas of ice subsidence beyond the lava flows indicate both thermal-related loss of ice, possibly related to minor meltwater drainage and physical collapse of ice adjacent to the lava flows (Figs. 10, 11). During our visits to the area in July and August, we observed no evidence for unusual outflow of water from the terminus of Cone Glacier (Fig. 1) and no sign of any glacier disruption except in the vicinity of the lava flows.

4.5 2018 eruption

The 2018 eruption is described in Waythomas et al. (2022) and Loewen et al. (2021) and is only briefly summarized here. Activity in 2018 began on September 3 with an increase in seismic tremor that typically indicates the onset of a new period of unrest (De Angelis and McNutt 2007). Low-level ash emissions were observed on September 4 and by September 7, low-level lava fountaining at cone A and small lava flows on the south flank of the cone were observed by web camera and in satellite images. Lava flows erupting from as many as four small vents on the south flank of cone A were observed in a WorldView-3 satellite image acquired on September 11, 2018 (Waythomas et al. 2022, Fig. 6). The September lava flows eventually covered an area of about 0.17 km² and had a minimum volume of at least $3 \times 10^{-4} \text{ km}^3$ (Waythomas et al. 2022). Photogrammetric data for a structure-from-motion digital elevation model (DEM) of the cone A area were obtained by the US Fish and Wildlife Service and the National Park Service on September 26, 2018 (Dietterich



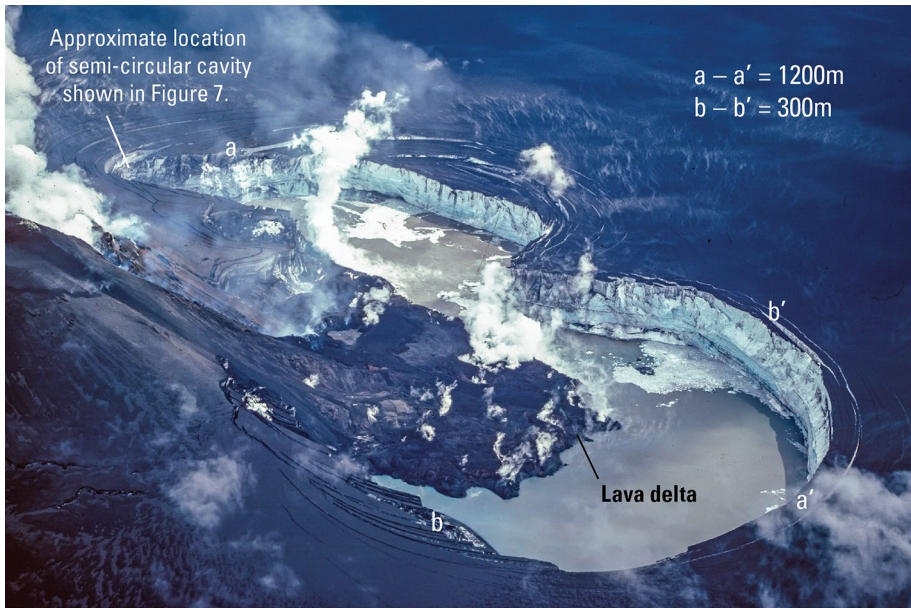


Fig. 6 Expanded glacier melt pit at the base of cone A, July 26, 1983. View is to the southeast. The distance from a–a' is about 1300 m, and the distance from b–b' is about 300 m; approximate area of the melt pit is 0.8 km². The lava flow visible in the center part of the photograph is mostly LF2. Photograph by E. Yount, 1983

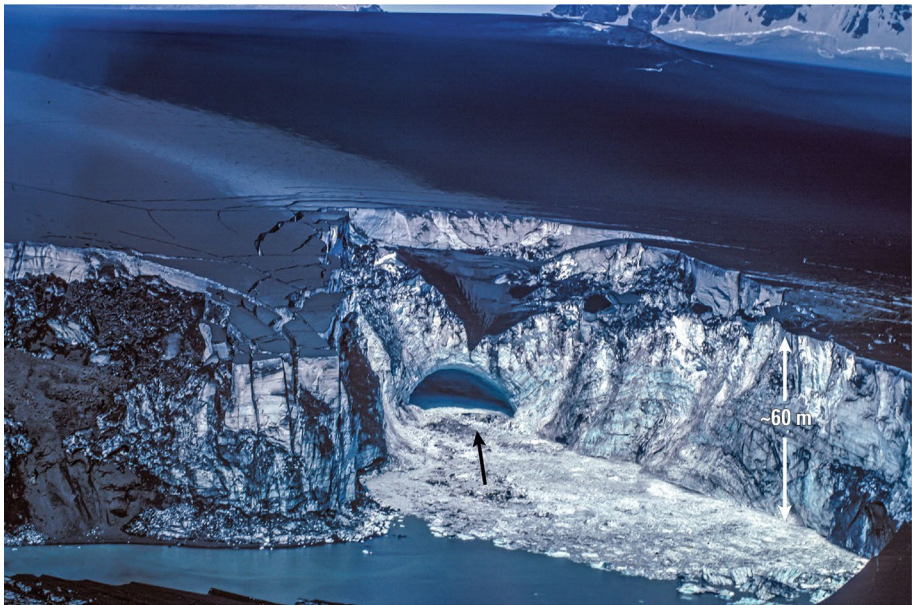


Fig. 7 Oblique aerial photograph of ice melt depression at the exposed base of Cone A, Veniaminof Volcano, July 13, 1983. The semicircular cavity in the middle of the photograph (black arrow) was probably formed by a lobe of lava flowing into the glacier and is not a subglacial meltwater tunnel as had been suspected when first observed. Approximate location of cavity shown on Fig. 6. Ice thickness estimated by Yount et al. 1985. Photograph by R. Emanuel, USGS

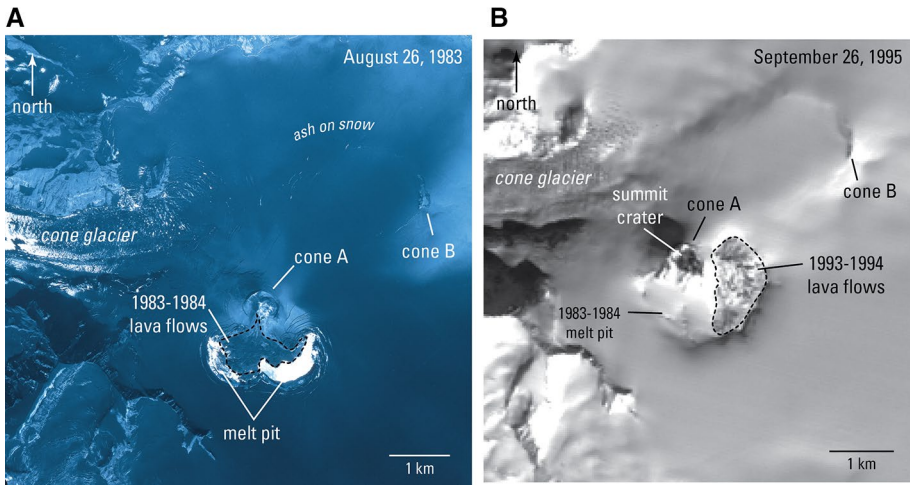


Fig. 8 Lava flows and melt features at cone A associated with the 1983–1984 (A) and 1993–1994 (B) eruptions. The vent for the subaerial lava flows of the 1983–1984 eruption was at the summit crater, whereas for the 1993–1994 eruption, lavas were erupted from a flank vent, southeast of the summit of cone A. Figure 8A is a US Geological Survey vertical color infrared aerial photograph taken on August 26, 1983 scale about 1:65,000. Figure 8B is a Landsat 5 image obtained on September 26, 1995, pixel resolution about 30 m

et al. 2021). These data were used to generate a DEM from which a shaded-relief map of the caldera was produced and used to portray the extent of lava flows as of September 26, 2018 (Fig. 12). Photographs taken during the September 26 overflight also showed the development of melt depressions peripheral to the lava flows and robust steaming along the lava flow margins where they were in direct contact with ice and snow (Fig. 13).

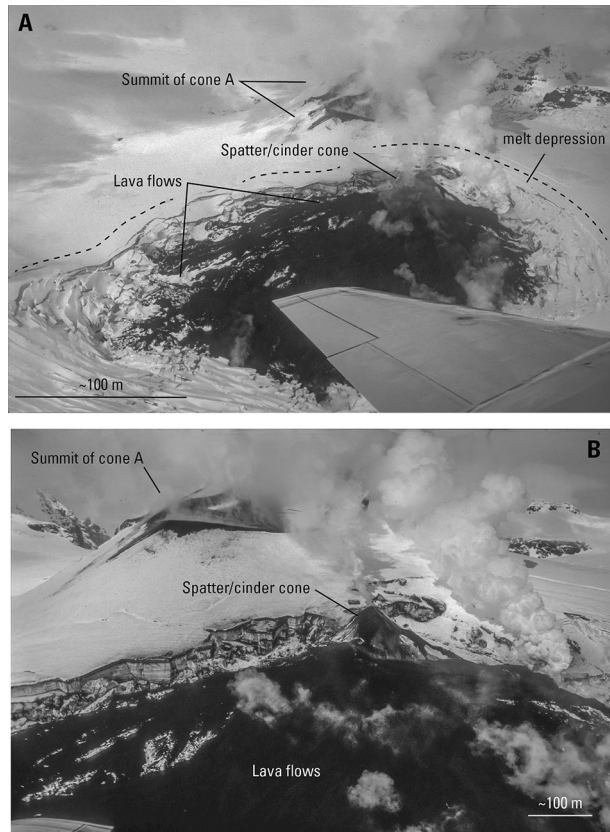
A WorldView satellite image obtained on October 3, 2018, showed continued advance of the lava flow, additional development of melted areas on the glacier, and expanded areas of concentric depressions just beyond the lava flows (Fig. 14). In this image, the lava flow covered an area of about 0.18 km². Robust steaming is apparent along the southeast margin of the flow, but ponded water is not obvious in the satellite image.

Intermittent lava effusion throughout October and early November increased the area of the flows to 0.37 km² as determined from a WorldView satellite image obtained on November 5 (Waythomas et al. 2022, Fig. 19). This image indicates that active lava flows were nested above previously emplaced flows which had partial snow cover. We note that the effusion of lava in October–November added to the cumulative lava thickness but likely did not enhance the heat flow to the underlying snow and ice on timescales significant to rapid meltwater production.

Cloud cover obscured Veniaminof Volcano and cone A until early December 2018 when a Sentinel-2 satellite image obtained on December 5 showed robust steaming associated with the advance of lava flows down the southeast and southwest flanks of cone A. By December 27, declining levels of seismic tremor and limited evidence for lava effusion in satellite data indicated that the eruption had ended.

The maximum extent of the 2018 lava flows is shown in a June 19, 2019, satellite image (Fig. 15). In this image the total area of the flows is about 0.6 km². The lava volume

Fig. 9 Lava flows and ice melt features on the southeast flank of cone A, May 9, 1994. In both photos, view is toward the north. **A** Oblique aerial view of lava flows, small cinder cone, and ice melt depression. The width of the lava flow field is about 200 m. **B** Closer in view of spatter/cinder cone and lava flows on the flank of cone A. Photos by C.J. Nye, Alaska Volcano Observatory



erupted in 2018 estimated by Loewen et al. (2021) is $6 \times 10^{-3} \text{ km}^3$ and the total ice loss is on the order of $0.014\text{--}0.003 \text{ km}^3$ (Table 2).

4.6 2021 eruption

The combination of elevated surface temperatures at cone A, detection of small, discrete explosions by infrasound sensors, and observations of ash emission in satellite and web camera images confirmed that low-level eruptive activity was underway by March 4, 2021. A high-resolution satellite image obtained on March 7, 2021, indicated that a subglacial vent about 1100 m east of cone A was erupting lava that resulted in the formation of a small ice cauldron (Fig. 16). By March 7, the ice cauldron was about 600 m long, 550 m wide and had an area of 0.26 km^2 . The March 7 satellite image also confirmed that minor explosive activity and ash emissions were occurring from the summit crater of cone A (Figs. 16, 17). Intermittent ash emission from the summit vent of cone A, explosions, and lava effusion at a cluster of three vents within the ice cauldron continued into late March when the eruption gradually ended. By early April 2021, three separate lava flows were visible on the floor of the ice cauldron. The maximum area of the ice cauldron was 0.67 km^2 as determined from an April 29, 2021, satellite image and the combined area of the lava flows was about 0.03 km^2 .

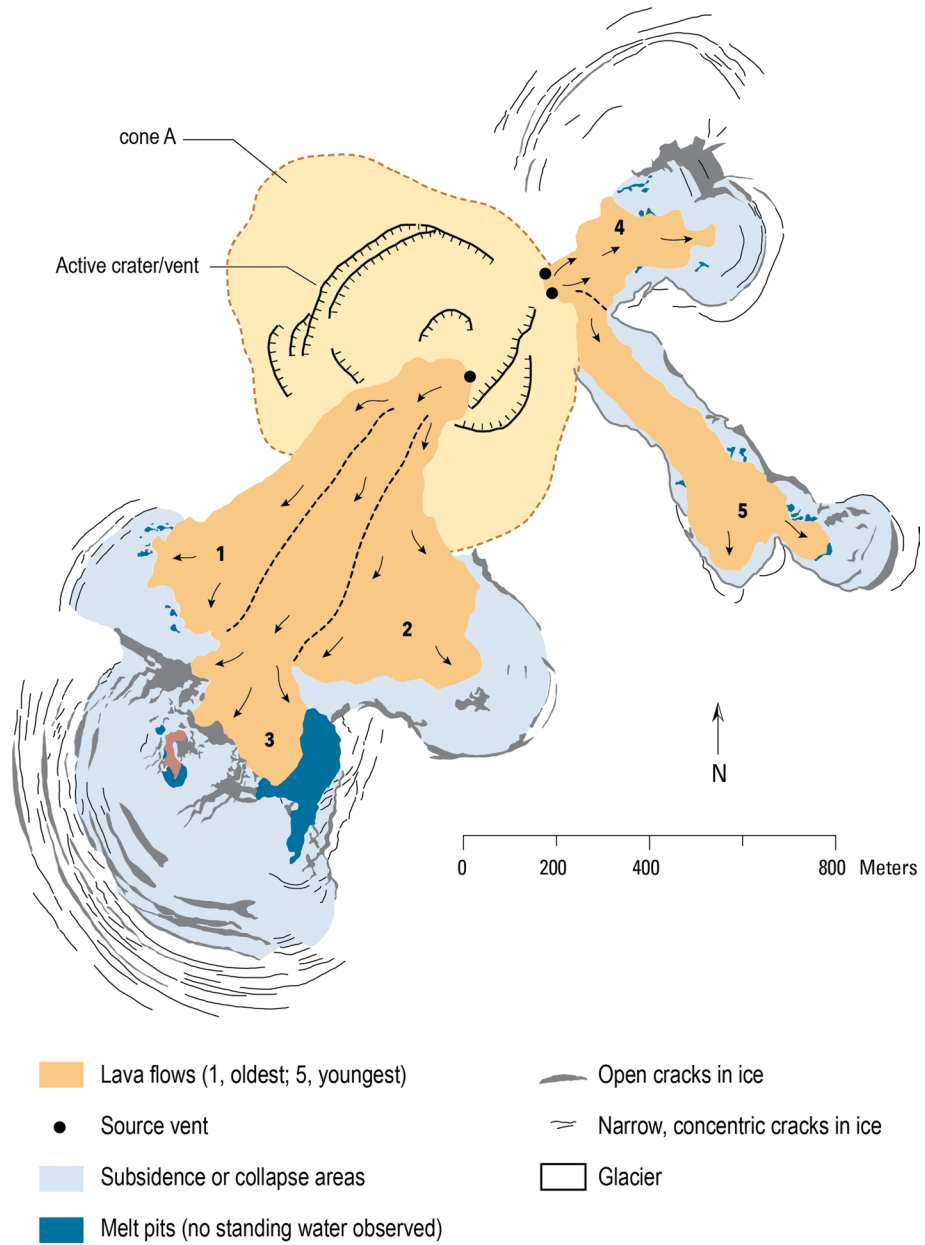


Fig. 10 Lava flows and ice subsidence features associated with the 2013 eruption of cone A. Map base is September 19, 2013, US Geological Survey satellite image; image resolution approximately 0.5 m

5 Supraglacial lava flows on ice and snow at Veniaminof Volcano

Lava flows erupted from cone A typically encounter snow and ice when the flows reach the lower third or so of the cone flank. Most of the theory described below pertains to lava

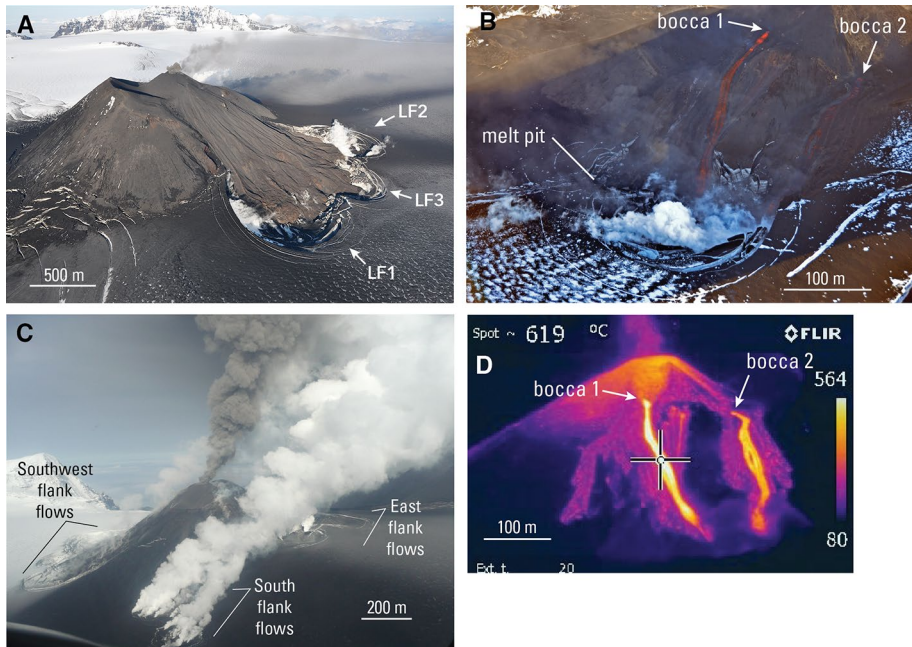


Fig. 11 Cone A at Veniaminof volcano in various states of activity during the 2013 eruption. **(A)** Lava flows 1, 2, and 3 and associated ice-melt depressions on the southwest flank of cone A. The distance from a–b is about 1 km and the height of cone A above the surrounding icefield is about 300 m. Photograph by R.G. McGimsey, August 18, 2013. **(B)** Incandescent lava flows and boccas (located by white arrows) on the east side of cone A. A bocca is an opening through which lava is effusing. Photograph by R.G. McGimsey, August 18, 2013. **(C)** Actively advancing lava flow on south flank of cone A. Also shown are lava flows on the southwest and east flanks of cone A. Photograph by J. Alto, September 7, 2013. **(D)** FLIR (Forward Looking Infrared Radiometer) image of the east side of cone A. A spot temperature measured on one of the lava flows indicated a temperature of about 619 °C, the highest temperature measured. Also note active warm emissions from the summit and a spatter collar around the top of the summit crater. Image by R.G. McGimsey, August 18, 2013

flows advancing over glacier ice, whereas at Veniaminof Volcano there is some amount of seasonal snow, firn, and ice that subaerial lava flows encounter around the base of cone A. Since we don't know the proportions or physical properties of snow, firn, and ice at this location we consider primarily lava-ice interactions. When a lava flow is extruded onto glacier ice (Fig. 18a), heat is transferred by conduction to the ice through the base of the flow and to the atmosphere from its exposed subaerial surface (Wilson and Head 2007; Edwards et al. 2012, 2015). If water can flow easily from the base of the flow, the temperature at the base of the lava flow rapidly approaches the melting point of ice (~ 273 K; Wilson and Head 2007). The cooling time of the lava is typically much longer than the duration of lava emplacement (Pinkerton and Wilson 1994; Harris and Rowland 2009), and thus, melting of snow and ice underlying the lava flow is a function of the long-term heat flux from the core of the flow through the lower part of the lava and into the ice substrate. The heat flux at the base of the lava flow (Q_b) can be expressed as

$$Q_b = -k \frac{dT}{dz} = k \frac{\Delta T}{\Delta z} \quad (1)$$

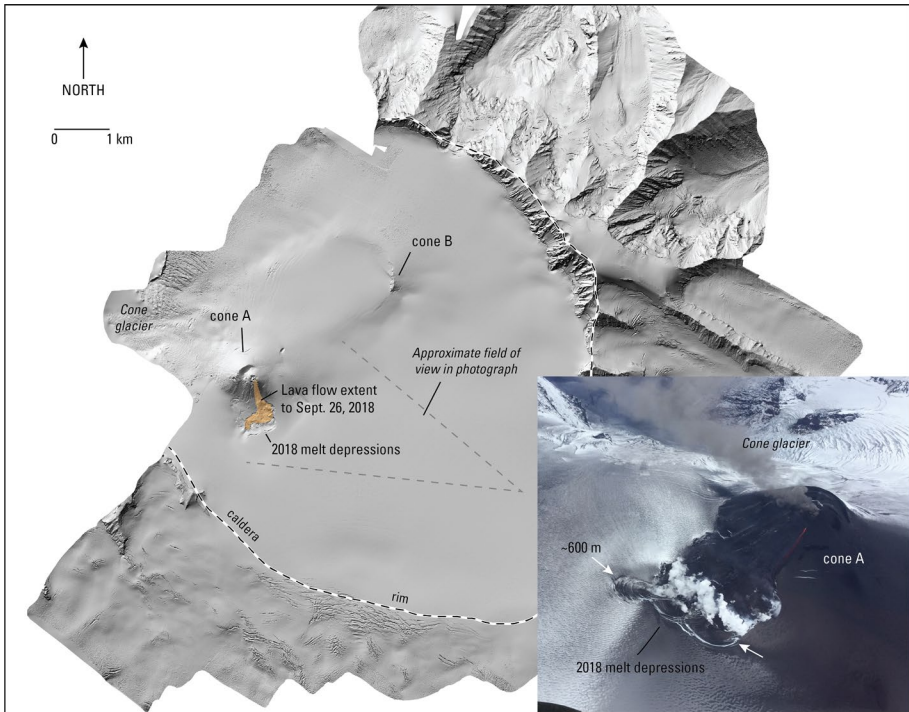


Fig. 12 Structure from motion digital elevation model-derived hillshade map of the summit area of Veniamonof Volcano. Data acquired September 26, 2018, by the U.S. Fish and Wildlife Service. Inset photograph by M. Laker, USFWS. Digital elevation model resolution is 0.58 m, root-mean-square error 2.3 m (Dietterich et al. 2021)

where k is the thermal conductivity of the lava and $\frac{dT}{dz}$ is the change in temperature with distance below the surface of the flow or another reference point. For one-dimensional steady-state conduction where the contact area is known, the expression becomes

$$Q_b = -kA \frac{T_2 - T_1}{L} \tag{2}$$

where A is the area of the lava flow, T_2 is the temperature of the base of the lava flow, T_1 is the temperature at the core of the lava flow, and L is the lava flow thickness (Fig. 18a). Calculations presented in Wilson and Head (2007) indicate that for basaltic lava flows on the order of 1–3 m thick, melt rates over the first 24 h after emplacement on glacier ice decline appreciably from $37\text{--}85 \times 10^{-6}$ m/s to about 6×10^{-6} m/s (Fig. 18a). For a 10-m-thick lava flow, the one-week melt rate ($\sim 3.14 \times 10^{-6}$ m/s) is not substantially different from that of a 3-m-thick flow (3.11×10^{-6} m/s) (Wilson and Head 2007).

To illustrate supraglacial lava flow melt rates at cone A, Eq. (2) is applied to a lava flow on the south flank of cone A visible in a satellite image from September 11, 2018 (Waythomas et al. 2022; Fig. 6). The lava flow in this image covered an area of about 5.06×10^{-2} km², and the flow was erupted over a 5-day period (September 7–11, 2018), giving an average daily area covered of 1.01×10^{-2} km². Using the 1.5-day melt rate for a 3-m-thick basaltic lava flow (6.8×10^{-6} m/s) calculated by Wilson and Head (2007), a lava

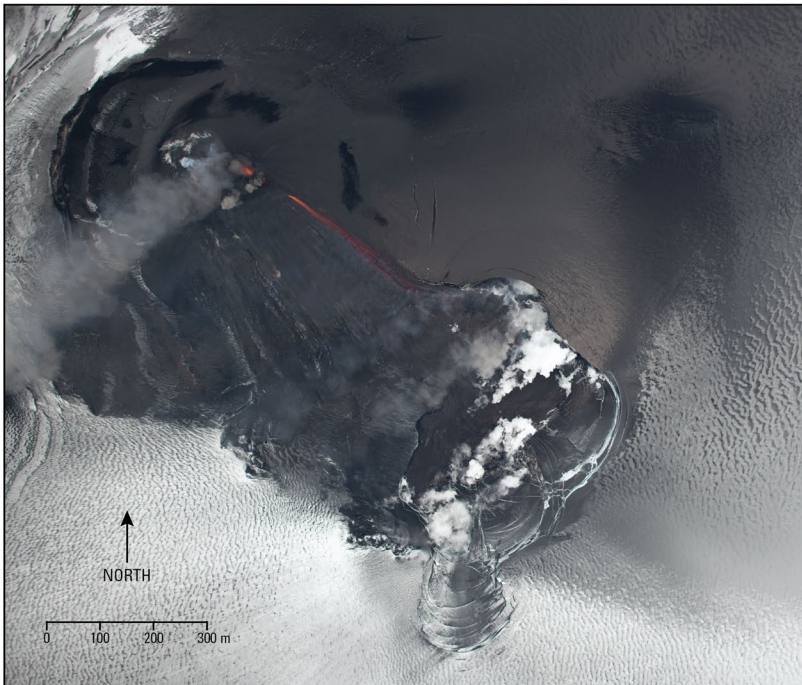
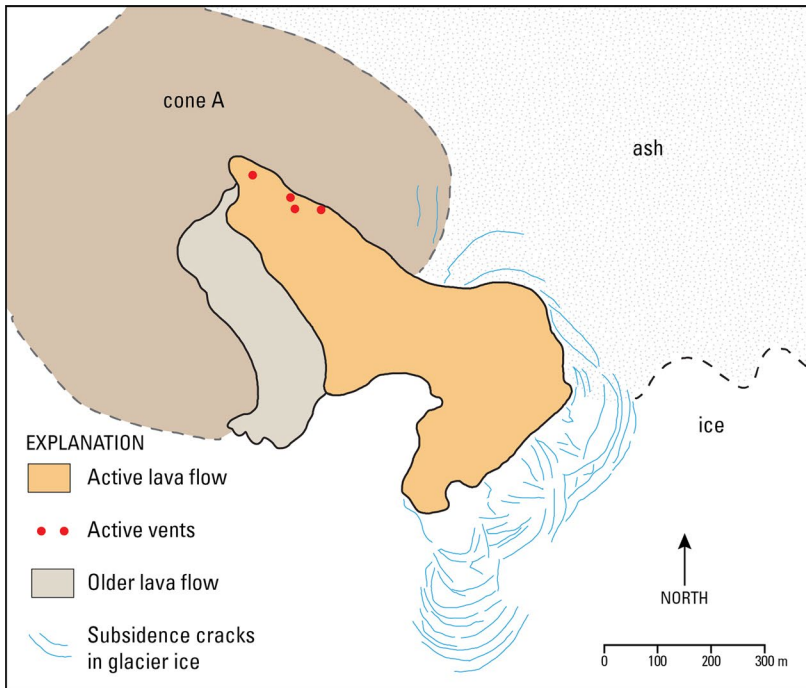


Fig. 13 Map and vertical aerial photograph of lava flows on the southeast flank of cone A, September 26, 2018. Photo by M. Laker, USFWS Lava flow area = 0.17 km²

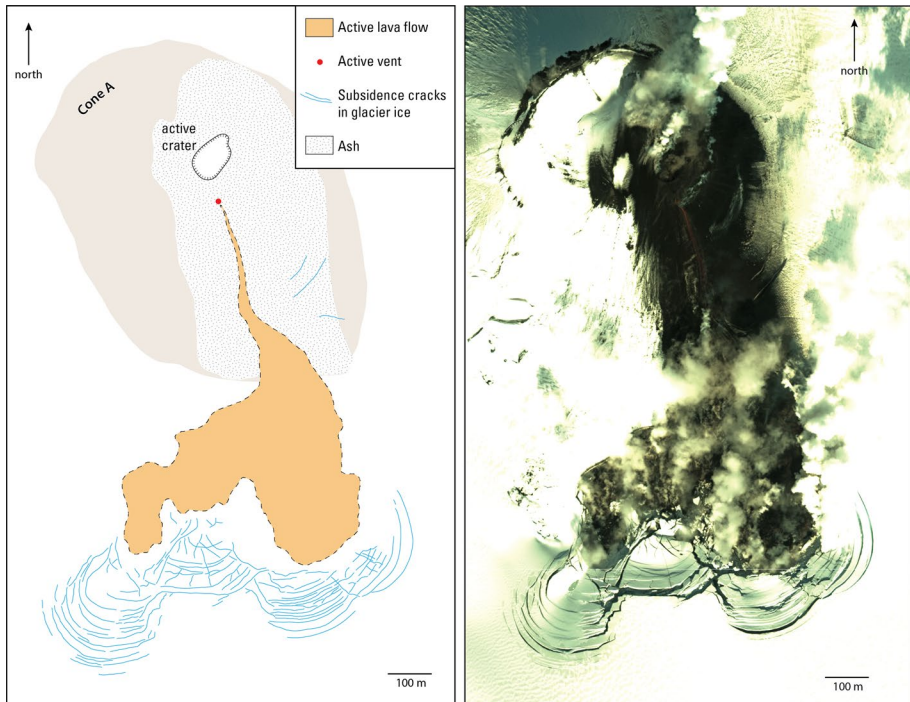


Fig. 14 Map and WorldView-3 satellite image of lava flows on the southeast flank of cone A, October 3, 2018. Lava flow area=0.18 km². Modified from Waythomas et al. 2022, Fig. 12

flow with an area of 10,120 m² gives an ice volume lost to melting of 6000 m³/d, which equates to about 5400 m³/d of meltwater or roughly 0.06 m³/s which is a low melt rate.

Lava flow melting of snow and firn also occurs as a result of heat conduction and radiation. Studies of the 2010 Fimmvörðuháls eruption, south-central Iceland, and the 2012–2013 Tolbachik eruption in Kamchatka showed that heat transfer by radiation was too low to cause significant melting of snow except in cases where lava flowed directly into steep walls of snow and ice (Edwards et al. 2012, 2015). As shown above, rates of heat conduction from the base of rubbly lava flows are low and observations at Tolbachik indicate that lava flows on the order of 2–3 m thick advancing over snow > 2 m thick did not produce rapid melting (Edwards et al. 2014).

The lava flow in the September 11, 2018, satellite image (Waythomas et al. 2022; Fig. 6) shows no evidence of significant ice or snow melt. The lava flow is about 680 m in length and if lava effusion began on September 7, the average flow rate from September 7 to 11 (5 days) is 136 m/d. Thus, it would take about 2.4 days for the flow to reach the base of cone A and begin flowing over snow and ice. At this rate of flow, the lava flow could have been over snow and ice for roughly 2.5 days yet showed no obvious signs of snow or ice melt. This observation suggests that there must have been a shallow thermal gradient from the core of the lava flow to its base. This was possibly the result of the development of an insulating basal breccia layer like those described by Edwards et al. (2012) during the 2010 Fimmvörðuháls eruption or like that portrayed ideally in Fig. 18a. The combined effects of an insulating basal breccia layer, underlying ash deposit, or both and the low thermal

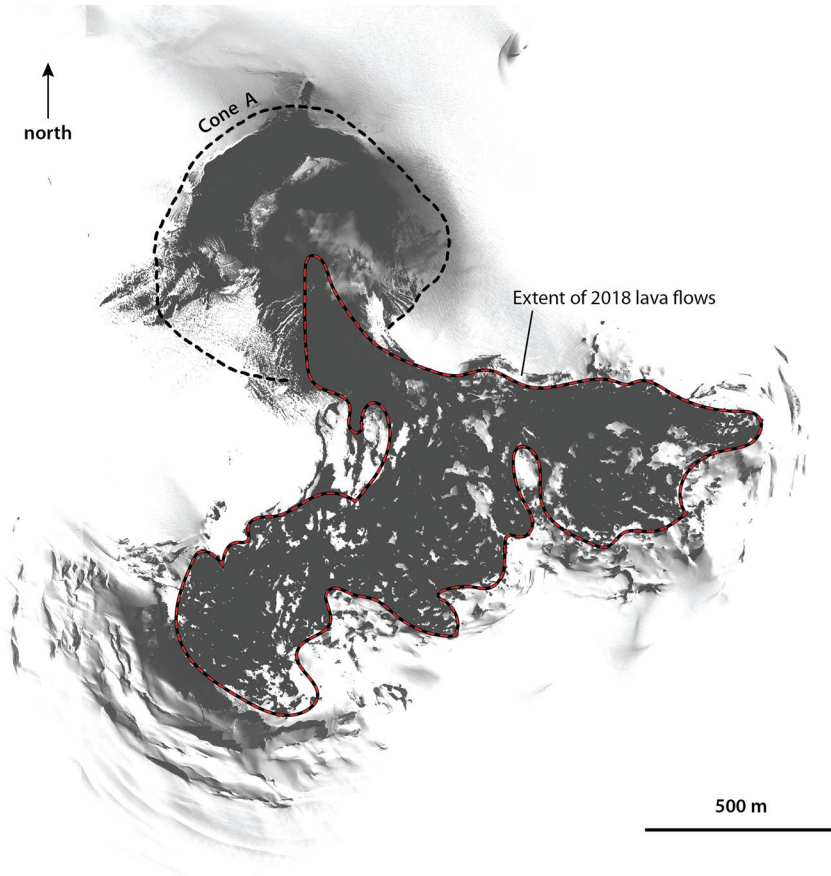


Fig. 15 WorldView-3 satellite image of cone A and the 2018 lava flows, as of June 19, about six months after the effusive phase of the eruption ended. Approximate lava area = 0.6 km^2

Fig. 16 Planet Labs satellite image from March 7, 2021, showing cone A in eruption and small ice cauldron about 1 km east of cone A. The ice cauldron has an area of about 0.26 km^2

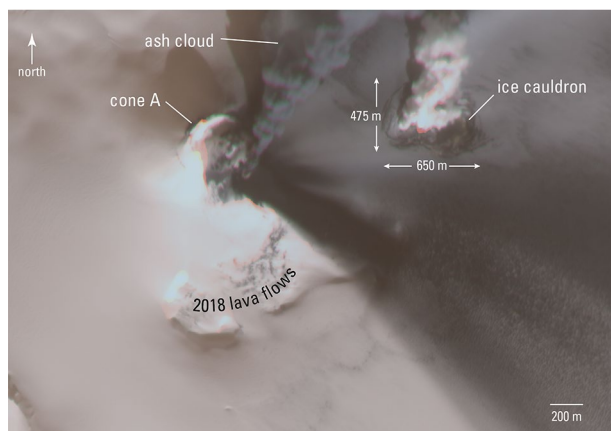


Table 2 Estimated ice loss associated with lava flow-ice interaction during historical eruptions of cone A at Veniaminof Volcano

Eruption	Estimated ice loss, in m ³	Comments
1944	Unknown	Steam plume and associated lava flow related melting observed in photograph (Fig. 4)
1983–1984	0.1	Based on maximum estimated dimensions of melt pit (800 x 1300 x 100 m)
1993–1994	0.024–0.004	Based on maximum dimensions of melt pit (800 x 1000 x 30–50 m; Neal et al. 1995)
2013	0.0025–0.01	Based on lava flow area (0.5 km ²) and inferred melt depth range of 5–20 m
2018	0.003–0.0134	Based on area of melted ice and melt depth range of 5–20 m
2021	0.003–0.0134	Based on area of ice cauldron (0.67 km ²) and inferred melt depth range of 5–20 m

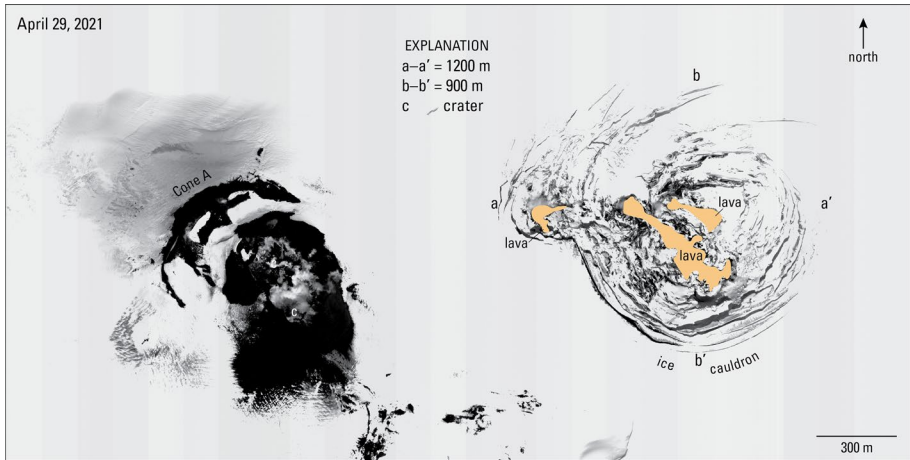


Fig. 17 WorldView-3 satellite image of ice cauldron and lava flows about 1 km east of cone (A), April 29, 2021. Note that the revised figure only has one part, not an A and B

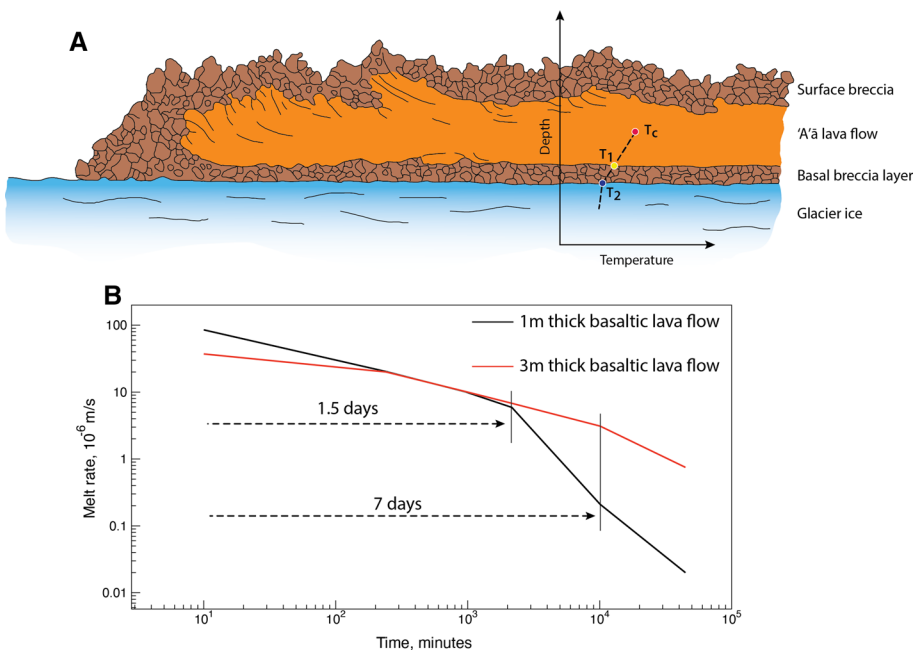


Fig. 18 (A) Schematic cross section of idealized cone A lava flow showing inner hot core, and exterior breccia layers (modified from Lockwood and Lipman 1980). Although the contact relations shown are flat lying, in most situations the surface slope is steeper and allows for meltwater to drain out ahead of the lava flow. The inset depth-temperature plot shows generalized thermal gradients from the core of the flow to the top of the glacier. See text for further discussion. (B) Glacier ice melt rate versus time for supraglacial basaltic lava flows 1 and 3 m thick. Data from Wilson and Head 2007

conductivity of air within the snowpack (DeWalle and Rango 2008) suggests that heat flux values at the lava-snow-ice interface should be low.

Most 'a' ā lava flows have rubbly surface and basal breccia layers (Fig. 18a; Lockwood and Lipman 1980) that modulate the heat flux from the lava flow core to the atmosphere and into the underlying substrate. The thickness, thermal, and rheological properties of basal breccia layers are not well known although there are theoretical treatments of the relevant physical properties (Kerr 2001; Harris 2013). Loock et al. (2010) suggested that in some settings, basal breccia layers, or basal clinker, may form by phreatomagmatic fragmentation, a process that likely occurs when lavas are extruded over ice and snow (Belousov et al. 2011). This process could temporarily increase the rate of meltwater generation due to the slightly greater surface area of interaction at the base of the flow. At present, we have no evidence to confirm or deny that this mechanism may operate at the cone A lava flows and have observed no evidence for phreatomagmatic explosions.

Minimal steaming around lava flow margins resting on snow were evident in aerial photographs of cone A taken on September 14, 2018. However, a satellite image obtained on September 16 clearly shows a prominent steam plume issuing from the terminus of the lava flow indicating melting was occurring by that time, approximately 6–7 days after lava reached snow and ice. Steaming around the margins of the lava flows became noticeable only after the flows gradually melted into the ice and had direct contact with ice walls or collapsed chunks of ice (Figs. 13, 14). Steam production likely occurs in these scenarios because the lava is in direct contact with ice for long enough for water to be converted to steam.

During all types of eruptive product interaction with ice and snow, the important factor with respect to potential lahar hazards is the rate of meltwater generation (Pierson et al. 1990; Thouret et al. 2007). Observations of the subaerial lava flows emplaced at cone A at Veniaminof Volcano indicate that the rate of meltwater generation is low relative to the timescale of lava flow emplacement and cooling. We conclude from these observations that supraglacial lava flows typically generated during effusive eruptions of cone A are unlikely to produce hazard-significant amounts of meltwater.

6 Subglacial lava effusion at Veniaminof Volcano

Subglacial lava effusion is generally uncommon at stratovolcanoes because their active vents are predominantly subaerial (Major and Newhall 1989). Effusion of lava beneath glacier ice is a process that has occurred historically at Veniaminof Volcano but is less common than supraglacial effusion of lava flows that extend over glacier ice. In general, lava flows emplaced subglacially are more efficient at melting glacier ice because about two thirds of the heat content of the lava is available to melt ice (Wilson and Head 2007). As a result, large volumes of ice can be melted in settings where glacier ice over the vent area is thick (> 100 m) as in Iceland (Gudmundsson et al. 2004). Subglacial lava eruptions in Iceland are often associated with the development of massive outburst floods (jökulhlaups) that can pose significant hazards in affected drainages (Björnsson 2003). The 1944, 1983–1984, 1993–1994, and 2021 eruptions at cone A all likely involved subglacial lava effusion.

Observations of the 1983–1984 eruption, as described previously, were sparse. Within approximately seven days after the start of the eruption in June 1983, a small circular ice cauldron, 1200 m long, 200–500 m wide, and 50–100 m deep was observed (Yount et al.

1985; Fig. 6). The analysis of glacier melt associated with subglacial lava effusion presented in Wilson and Head (2007) indicates that the ratio of ice thickness melted to subglacial lava thickness is 6–7. If a 100 m deep ice cauldron formed entirely by subglacial melting, the ratio indicates that a subglacial lava flow 14–17 m thick could have been present beneath the glacier. The study by Loewen et al. (2021) indicated that the lava flows erupted in 2018 were on the order of 3–15 m thick, so this ratio seems at least qualitatively plausible. In general, the flows emplaced in 2018 are comparable in extent to the lavas emplaced during previous historical eruptions implying that the 1983 lavas may have been at least locally as much as 15 m thick.

Photographs of the ice cauldrons near cone A (Figs. 5, 17) show extensive crevassing indicating that the glacier is undergoing brittle deformation. The crevasse depth provides an approximation of the thickness of the brittle part of the glacier above a presumed ductile zone that is expected to deform according to Glen’s flow law for ice (Cuffey and Paterson 2010). The crevasse depth (d) is related to the horizontal strain rate of ice ($\dot{\epsilon}_{xx}$) according to the following expression:

$$d = \frac{2}{\rho_i g} \left(\frac{\dot{\epsilon}_{xx}}{A} \right)^{1/n} \tag{3}$$

where ρ_i is ice density, g is gravitational acceleration, A is a temperature-dependent flow law parameter ($2.4 \times 10^{-24} \text{ s}^{-1} \text{ Pa}^{-3}$ at 0 °C, Cuffey and Paterson 2010), and $n=3$ (Nye 1957). Although $\dot{\epsilon}_{xx}$ is not known for Veniaminof’s glaciers, we use a typical value of 10^{-8} s^{-1} (Cuffey and Paterson 2010). Application of Eq. (3) indicates that the theoretical crevasse depths are greater than the ice thickness (about 100 m; Welch et al. 2007). Although Eq. 3 is shown to overestimate crevasse depths by as much as 15% (Mottram and Benn 2009), the implication is that all ice affected by subglacial lava effusion at Veniaminof Volcano likely behaves in a brittle fashion and there is little if any ductile flow of ice to the eruption site.

The crevasse fields peripheral to cone A lava flows in general extend 200–500 m beyond lava flow termini (Figs. 12, 13, 14). If the development of crevasses reflects loss of ice beneath the crevasse field and subsequent brittle subsidence, the extent of these fields likely records the flow of warm meltwater away from the lava flows.

For temperate glaciers, the heat lost (Q) due to melting by subglacial lava flows can be expressed as

$$Q = \rho_i V_i L_i \tag{4}$$

(Gudmundsson 2000) where ρ_i is ice density, V_i is ice volume lost, and L_i is the latent heat of fusion of ice (334 kJ/kg). The density of glacier ice at 0 °C is 917 kg/m³ and the estimated volumes of ice lost in 1983–1984 and 2021 are 0.1 and 10^{-3} km^3 , respectively. This equates to about 0.09 km³ of water for the 1983–1984 eruption and $9 \times 10^{-4} \text{ km}^3$ of water for the 2021 eruption. Application of Eq. (4) indicates that the heat energy required to form the melt pits was $3 \times 10^{16} \text{ J}$ for the 1983–1984 eruption and $3 \times 10^{14} \text{ J}$ for the 2021 eruption.

If we assume that the melt pits formed in 1983–1984 and 2021 were entirely the result of subglacial lava effusion, the volume of magma (V_m) involved can be estimated with the following expression:

$$V_m = \frac{\rho_i L_i V_i}{\rho_m C_m \Delta T} \tag{5}$$

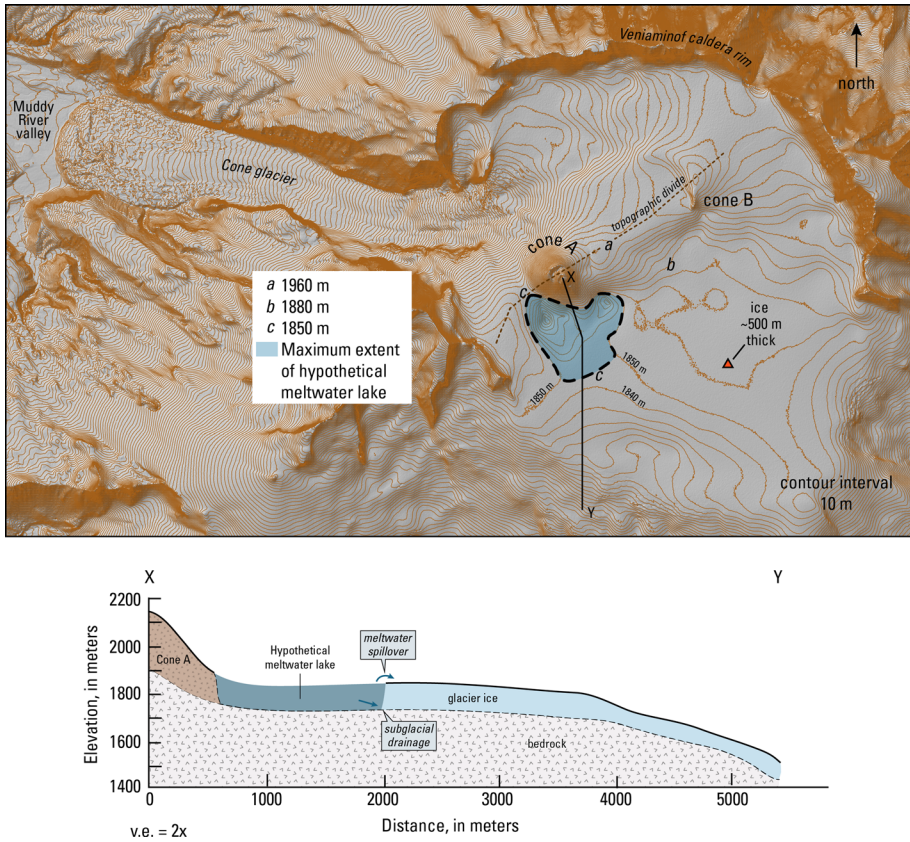


Fig. 19 Topographic map and cross section of area south of cone A at Veniaminof volcano showing maximum extent of hypothetical meltwater lake. Digital elevation data from DGGs Staff, 2013, Elevation Data-sets of Alaska. Alaska Division of Geological and Geophysical Surveys Digital Data Series 4, <https://elevation.alaska.gov/>. <https://doi.org/10.14509/25239>

where ρ_i , L_i , and V_i are as defined above, and ρ_m is magma density (2600 kg/m^3), C_m is the specific heat capacity of volcanic glass ($1.1 \text{ kJkg}^{-1} \text{ K}^{-1}$ (Bacon 1977)), and ΔT is the temperature difference between the initial magma (T_m) and the ambient temperature (T_s) such that $\Delta T = T_m - T_s$ (Gudmundsson et al. 2004). Using 1173 K for T_m , and 273 K for T_s , $\Delta T = 900 \text{ K}$. Alternatively, if no quenching occurs and the specific heat capacity of crystalline basalt is used in the denominator ($\rho_m [L_m + C_p \Delta T]$) where $C_p \sim 0.6 \text{ kJ kg}^{-1} \text{ C}^{-1}$, the result is about the same. Application of Eq. (5) indicates theoretical subglacial lava volumes of 0.01 km^3 for the 1983–1984 eruption and 10^{-4} km^3 for the 2021 eruption. These values do not account for any subaerial effects on melting which would be minor, or the melting associated with the long cooling time of the lava flows and thus should be viewed as minimum estimates.

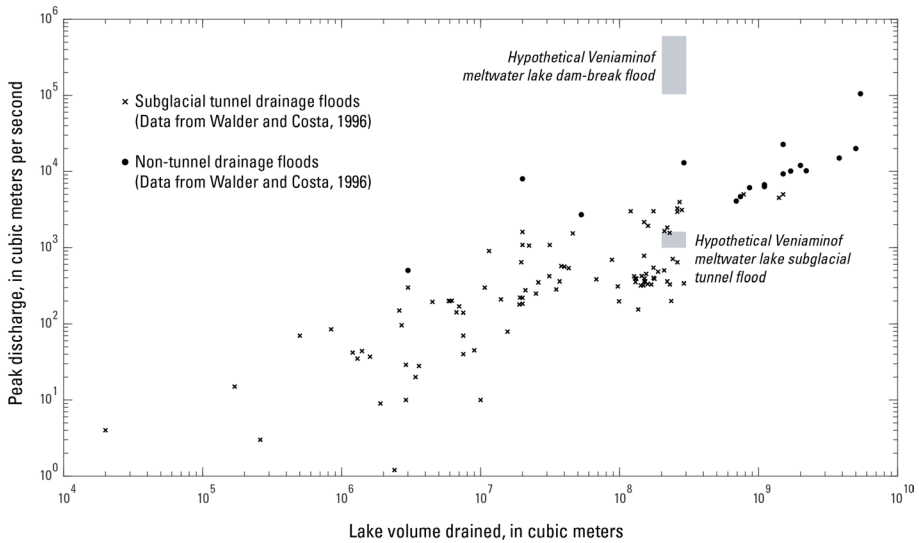


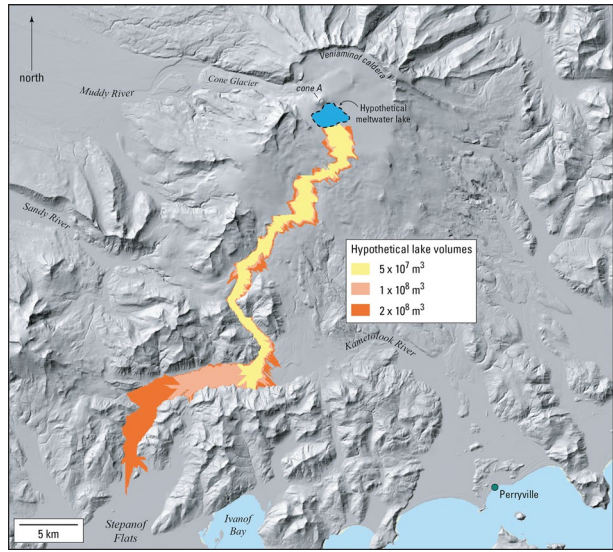
Fig. 20 Lake volume drained versus peak discharge for glacier-dammed lakes that drain by evolution of subglacial tunnels and by failure of associated ice dams (Data from Walder and Costa 1996). Failure of a hypothetical meltwater lake dam at Veniaminof volcano could produce a large outburst flood. Subglacial tunnel drainage of a hypothetical meltwater lake has an associated peak discharge similar to lakes with equivalent volumes

7 Meltwater lakes and associated flood and lahar hazards

Given the large volume of glacier ice resident on Veniaminof Volcano edifice and the frequency of historical eruptions, it is important to consider the potential for eruption generated flood and lahar hazards in the main drainages beyond the caldera. Eruptions in 1983–1984, 1993–1994, 2013 and 2018 all resulted in the formation of lava flows that extended over ice and snow just beyond the base of cone A. The ice-radar survey results (Welch et al. 2007) and the recently available IfSAR digital elevation data for Veniaminof show a topographic ridge oriented roughly northeast-southwest between cones A and B (Fig. 19). This ice-covered ridge is a barrier to water flow and appears to prevent meltwater from entering the Cone Glacier–Muddy River drainage. It is possible that if lava effusion occurred on the north side of cone A, meltwater could plausibly leak into the Cone Glacier–Muddy River drainage. However, we have no evidence that any historical eruptions have produced lava flows on this side of the cone.

If a hypothetical meltwater lake was to form in the area of lava flow emplacement south of cone A, it could cover a maximum area of about 2 km² before it spilled over the low point along the southwest rim of the caldera where the maximum surface elevation of the lake would be about 1850 m (Fig. 19). For a meltwater lake with this area and a depth of 50–100 m, the volume would be 0.1–0.2 km³. Assuming that such a lake was the product of subglacial lava effusion only, subglacial lava flows on the order of 7–8 m thick would be required to melt a 50 m thickness of ice and lava flows 14–16 m thick would be needed to melt ice 100 m thick (Wilson and Head 2007). The corresponding lava flow volumes would have volumes of roughly 0.01 km³, considerably more voluminous than any of the lava flows produced at Veniaminof since 1944. There are several plausible scenarios for

Fig. 21 Areas that could be inundated by lahars associated with catastrophic drainage of a hypothetical meltwater lake (shown in Fig. 20) near cone A at Veniaminof volcano. Inundation areas were determined with LaharZ, a GIS-based lahar inundation mapping tool (Schilling 2014)



drainage of such a lake including (1) seepage of water into the volcanic edifice, (2) subglacial tunnel drainage, or (3) spillover of water at the low point of the ice dam and possible catastrophic breaching.

Instantaneous failure of an ice dam would theoretically produce the largest peak discharge (Q_p) at the breach (Walder and Costa 1996). For rapid breach formation to the full depth of the meltwater lake, the expression for maximum peak discharge is

$$Q_p = 1.94g^{\frac{1}{2}}d^{\frac{5}{2}} \tag{6}$$

where g is gravitational acceleration and d is water depth at the breach (Waythomas et al. 1996). Application of this equation to the hypothetical meltwater lake at Veniaminof gives estimates of Q_p of $1-6 \times 10^5 \text{ m}^3/\text{s}$ for water depths of 50 and 100 m (Fig. 20).

Catastrophic breaching of an ice dam involving this hypothetical meltwater lake could produce a significant lahar. The theoretical area of inundation was estimated using a geographic information system (GIS)-based lahar inundation mapping tool known as LaharZ (Iverson et al. 1998; Schilling, 2014). LaharZ makes use of a physically based relation between lahar volume (V) and planimetric area of inundation (B) such that

$$B = 200V^{2/3} \tag{7}$$

Inundation areas for lahars arising from catastrophic drainage of hypothetical meltwater lakes with volumes of 0.05, 0.1, and 0.2 km^3 are shown in Fig. 21. These flows could travel approximately 35–40 km downstream from the breach in unnamed valleys on the southwest flank of Veniaminof where they could inundate an area as much as 67 km^2 .

If lake drainage was to occur through a subglacial tunnel (which we consider unlikely), the maximum peak discharge (Q_p) can be estimated with the following equation:

$$Q_p = 46V^{0.66} \tag{8}$$

where V is lake volume drained (Walder and Costa 1996). Application of this equation to the hypothetical meltwater lake at Veniaminof gives a Q_p of $1\text{--}1.5 \times 10^3$ m³/s. If the meltwater lake that formed during the 1983–1984 eruption drained via subglacial tunnel drainage according to this equation, $Q_p = 290$ m³/s. The above relation is a regression equation based on data compiled in Walder and Costa (1996; Fig. 20) and estimates of peak discharge should be taken as order of magnitude estimates only.

8 Discussion

The observations we have assembled indicate that cone A lava flows at Veniaminof Volcano interact with snow and ice by conduction at the lava-ice interface and produce small but not negligible amounts of ice loss (Table 2). Melting of ice and snow by the advancing supraglacial lavas resulted in gradual downward sinking of the lava flows into the ice, accompanied by local collapse of melt pit walls forming a jumble of ice blocks below. The characteristics of lava-flow bases at the lava-ice interface are not known, but it is likely that chilled, fractured, or rubbly basal zones developed rapidly and this likely decreased the heat flow from the still hot core of the lava flow to the underlying ice and snow. The transfer of heat from the base of the lava flow to the ice is a relatively inefficient mechanism for melting hazard-significant amounts of ice and snow because of rapid cooling and development of a “chilled” and fractured lava flow base especially in situations where the lava advances slowly over snow and ice (Mee et al. 2006; Belousov et al. 2011; Edwards et al. 2012). Limited meltwater production also has been confirmed in theoretical analyses (Wilson and Head 2007) and experimental studies (Edwards et al. 2013). If lava advances over snow and ice on steeper slopes, observations from Fimmvörðuháls indicate that greater amounts of melting may be facilitated by meltwater “degrading” the snow and ice cover out ahead of the advancing flow (Edwards et al. 2012). Ice subsidence areas peripheral to cone A lava flows indicate that this process also occurs at Veniaminof Volcano. Brief periods of robust steaming observed in web camera views and aerial photographs indicate that advancing lava flows were incorporating snow and possibly ice at the flow margins. The interactions may have been like the lava, snow and ice interactions at Nevados de Chillan, Chile (Mee et al. 2006), and Fimmvörðuháls, Iceland (Edwards et al. 2012) where slow downward melting or thermal sinking of the lava occurred as a result of heat exchange by conduction and radiation.

Historical eruptions of cone A indicate that this style of eruption is unlikely to lead to the generation of large amounts of meltwater. Future lava-producing eruptions at this volcano, if similar to recent historical eruptions, are not likely to cause significant lahar or flood events in the outlet drainages heading on the ice-filled caldera. Significantly more explosive eruptions, especially those that produce pyroclastic flows, would likely generate larger volumes of meltwater and could result in inundation of local valleys and drainages on the flanks of the volcano. Sustained subglacial effusive activity could lead to the development of a large meltwater lake and result in significant floods and lahars if such a lake drained by catastrophic failure of its ice dam (Fig. 21). Historically, no known lava flows have developed on the north side of cone A and there is no geomorphic evidence for water outflow in the Cone Glacier—Muddy River drainage to the north (for example, no flood deposits or unusual hydrologic features commonly associated with extreme flooding). Lahar deposits of Holocene age are preserved in many of the main valleys on the volcano, but these are associated with the large caldera-forming eruption that occurred ca. 3.7 ka

(Miller et al. 2002; Waythomas et al. 2015). Geomorphic evidence for young lahars or floods associated with outflow of meltwater from the caldera is not known at Veniaminof Volcano.

9 Conclusions

Cone A, a 300-m-high intracaldera cinder cone within the 8×10 km diameter caldera ice-field of Veniaminof Volcano has been the site of at least 20 eruptions since 1830–1840. Five of these eruptions in 1944, 1983–1984, 1993–1994, 2013, and 2018 involved supraglacial lava effusion, although the initial effusion of lava in 1983–1984 was subglacial. Lava effusion during the 2021 eruption was entirely subglacial. Except for the 2021 eruption, each of these eruptions produced $>10^{-4}$ km³ of lava and melted about $3\text{--}14 \times 10$ km³ of ice, except the 1983–1984 eruption where as much as 0.1 km³ of ice was melted. The lack of reliable field measurements on depth of ice melt, ice temperature, lava boundary layer properties, proximal ash thickness, and lava temperatures precludes a more robust analysis of the thermodynamics of lava-ice interaction at Veniaminof Volcano. Quantities of meltwater sufficient to pose a significant outflow flood hazard during the type of activity described here is not an outcome of lava-snow-ice interaction. Significant lahar hazards could arise if a large meltwater lake develops in the caldera and its contents are released rapidly by catastrophic breaching of its ice dam. To date, we have no evidence that this type of hydrologic hazard has occurred during historical eruptions at Veniaminof Volcano.

Acknowledgements The site visit to the 2013 eruption site was funded in part by National Geographic Research Committee Grant #9356-13 to BRE. BRE also thanks T. Neal for calling his attention to the 2013 eruption, and to AVO staff for hosting his quick visit to Anchorage in preparation for that fieldwork. The authors wish to thank Kristi Wallace, Tim Orr, Michelle Coombs (all USGS), Rosie Cole and an anonymous reviewer for their thoughtful reviews and comments on the manuscript. Any use of trade, firm, or product names is for descriptive purposes only and does not imply endorsement by the U.S. Government.

Open Access This article is licensed under a Creative Commons Attribution 4.0 International License, which permits use, sharing, adaptation, distribution and reproduction in any medium or format, as long as you give appropriate credit to the original author(s) and the source, provide a link to the Creative Commons licence, and indicate if changes were made. The images or other third party material in this article are included in the article's Creative Commons licence, unless indicated otherwise in a credit line to the material. If material is not included in the article's Creative Commons licence and your intended use is not permitted by statutory regulation or exceeds the permitted use, you will need to obtain permission directly from the copyright holder. To view a copy of this licence, visit <http://creativecommons.org/licenses/by/4.0/>.

References

- Bacon CR (1977) High temperature heat content and heat capacity of silicate glasses: experimental determination and a model for calculation. *Am J Sci* 277:109–135
- Bacon CR, Calvert AT, Nye CJ, Sisson TW (2003) History and eruptive style of Veniaminof Volcano, a huge Alaskan basalt-to-dacite volcano with Pleistocene and Holocene caldera-forming eruptions. *Eos* 84(46):V32D-1048
- Barr ID, Lynch CM, Mullan D, De Siena L, Spagnolo M (2018) Volcanic impacts on modern glaciers: a global synthesis. *Earth Sci Rev* 182:186–203. <https://doi.org/10.1016/j.earscirev.2018.04.008>
- Belousov A, Behncke B, Belousova M (2011) Generation of pyroclastic flows by explosive interaction of lava flows with ice/water-saturated substrate. *J Volcanol Geotherm Res* 202:60–72
- Björnsson H (2003) Subglacial lakes and jökulhlaups in Iceland. *Glob Planet Change* 35(3):255–271
- Calvert AT, Bacon CR, Sisson TW (2005) Argon geochronology of lavas at Mt. Veniaminof volcano dates pleistocene climatic events on the alaska peninsula. *AGU Fall Meet Abstr* 2005:V13D-0573

- Calvert AT, Bacon CR, Sisson TW (2021) Compositional progression from basalt-only to basalt+andesite+dacite during the 300 ka eruptive history of Mt. Veniaminof. *Alaska Geological Society of America Abstracts with Programs*, vol 53, no 6
- Cuffey KM, Paterson WSB (2010) *The physics of glaciers*. Academic Press, New York
- Delgado Granados H, Julio Miranda P, Ontiveros González G, Cortés Ramos J, Carrasco Núñez G, Pulgarín Alzate B et al (2015) Hazards at Ice-clad volcanoes: phenomena, processes, and examples from Mexico, Colombia, Ecuador, and Chile. In: Haeberli W, Whiteman C (eds) *Snow and ice-related hazards, risks, and disasters*. Elsevier, Amsterdam, pp 607–646
- Detterman RL, Miller TP, Yount ME, Wilson FH (1981) Quaternary geologic map of the Chignik and Sutwik Island quadrangles, Alaska. *US Geol Surv Misc Inv Ser Map I:1292*
- De Angelis S, McNutt SR (2007) Observations of volcanic tremor during the January–February 2005 eruption of Mt. Veniaminof, Alaska. *Bull Volcanol* 69(8):927–940
- DeWalle DR, Rango A (2008) *Principles of snow hydrology*. Cambridge Univ Press, Cambridge
- Dietterich HR, Loewen MW, Laker M, Orr T, Hulst C (2021) Digital elevation models and orthoimagery from the 2018 eruption of Veniaminof, Alaska. *US Geol Surv data release*. <https://doi.org/10.5066/P9VEFFRX>
- Dixon JP, Cameron C, McGimsey RG, Neal CA, Waythomas C (2015) 2013 Volcanic activity in Alaska - Summary of events and response of the Alaska Volcano Observatory: U.S. Geological Survey Scientific Investigations Report 2015-5110, pp 92. <https://doi.org/10.3133/sir20155110>
- Edwards BR, Belousov A, Belousova M (2014) Propagation style controls lava-snow interactions. *Nat Commun*. <https://doi.org/10.1038/ncomms6666>
- Edwards BR, Belousov A, Belousova M, Melnikov D (2015) Observations on lava, snowpack and their interactions during the 2012–13 Tolbachik eruption, Klyuchevskoy Group, Kamchatka, Russia. *J Volcanol Geoth Res*. <https://doi.org/10.1016/j.jvolgeores.2015.08.010>
- Edwards B, Kochitzky W, Battersby S (2020) Global mapping of future glaciovolcanism. *Glob Planet Change* 195:103356. <https://doi.org/10.1016/j.gloplacha.2020.103356>
- Edwards BR, Karson J, Wysocki R, Lev E, Bindeman I, Kueppers U (2013) Constraints on lava–ice interactions from large scale experiments. *Geology* 41:851–854
- Edwards B, Magnússon E, Thordarson T, Guðmundsson MT, Höskuldsson A, Oddsson B, Haklar J (2012) Interactions between lava and snow/ice during the 2010 fimmvörðuháls eruption south-central Iceland. *J Geophys Res Solid Earth*. <https://doi.org/10.1029/2011JB008985>
- Guðmundsson MT, Sigmundsson F, Björnsson H, Högnadóttir T (2004) The 1996 eruption at gjálp, vatnajökull ice cap, Iceland: efficiency of heat transfer, ice deformation and subglacial water pressure. *Bull Volcanol* 66(1):46–65. <https://doi.org/10.1007/s00445-003-0295-9>
- Guðmundsson MT (2000) Melting of ice by magma-ice-water interactions during subglacial eruptions as an indicator of heat transfer in subaqueous eruptions. In: White JDL, Smellie JL, Clague DA (eds) *Explosive subaqueous volcanism*. American Geophysical Union Geophysical Monograph Series, vol 140, pp 61–72. Doi: <https://doi.org/10.1029/140GM04>
- Haney MM (2014) Back projection of volcanic tremor. *Geophys Res Lett* 41(6):1923–1928. <https://doi.org/10.1002/2013GL058836>
- Harris AJL (2013) Lava flows. In: Fagents SA, Gregg TKP, Lopes RMC (eds) *Modeling volcanic processes: the physics and mathematics of volcanism*. Cambridge University Press, New York, pp 85–106
- Harris AJL, Rowland SK (2009) Effusion rate controls on lava flow length and the role of heat loss: a review. *Studies in volcanology: the legacy of George Walker*. *Spec Publ IAVCEI* 2:33–51
- Heiken G, Wohletz K (1985) *Volcanic ash*. University of California Press, Berkeley
- Iverson RM, Schilling SP, Vallance JW (1998) Objective delineation of lahar-inundation hazard zones. *Bull Geological Soc Am* 110(8):972–984. [https://doi.org/10.1130/0016-7606\(1998\)110%3c0972:ODOLIH%3e2.3.CO;2](https://doi.org/10.1130/0016-7606(1998)110%3c0972:ODOLIH%3e2.3.CO;2)
- Kerr RC (2001) Thermal erosion by laminar lava flows. *J Geophys Res Solid Earth* 106(B11):26453–26465
- Lockwood JP, Lipman PW (1980) Recovery of datable charcoal beneath young lavas: lessons from Hawaii. *Bull Volcanol* 43(3):609–615. <https://doi.org/10.1007/BF02597697>
- Loewen ML, Dietterich HR, Graham N, Izbekov P (2021) Evolution in eruptive style of the 2018 eruption of Veniaminof volcano, Alaska, reflected in groundmass textures and remote sensing. *Bull Volcanol* 83(72):19. <https://doi.org/10.1007/s00445-021-01489-6>
- Look S, de Vries BVW, Hénot JM (2010) Clinker formation in basaltic and trachybasaltic lava flows. *Bull Volcanol* 72(7):859–870. <https://doi.org/10.1007/s00445-010-0362-y>
- Major JJ, Newhall CG (1989) Snow and ice perturbation during historical volcanic eruptions and the formation of lahars and floods. *Bull Volcanol* 52(1):1–27
- McGimsey RG, Neal CA, Doukas MP (1995) Volcanic activity in Alaska: summary of events and response of the Alaska Volcano Observatory 1992. *US Geol Surv Open-File Report* 26:95–83

- Mee K, Tuffen H, Gilbert JS (2006) Snow-contact volcanic facies and their use in determining past eruptive environments at Nevados de Chillán volcano. *Chile Bull Volcanol* 68(4):363–376. <https://doi.org/10.1007/s00445-005-0017-6>
- Miller TP, McGimsey RG, Richter DH, Riehle JR, Nye CJ, Yount ME, Dumoulin JA (1998) Catalog of the historically active volcanoes of Alaska. US Geol Surv Open-File Report OF 104:98–0582
- Miller TP, Waythomas CF, Gardner JE (2002) Possible multiple late Quaternary caldera-forming eruptions at Mount Veniaminof Volcano, Alaska Peninsula. *Eos Trans AGU* 83(47):V11A-1376
- Miller TP, Smith RL (1987) Late Quaternary caldera-forming eruptions in the eastern Aleutian arc Alaska. *Geology* 15(5):434–438
- Mottram RH, Benn DI (2009) Testing crevasse-depth models: a field study at Breiddöamerkurjökull. *Icel J Glaciol* 55(192):746–752. <https://doi.org/10.3189/002214309789470905>
- Neal CA, Doukas MP, McGimsey RG (1995) 1994 volcanic activity in Alaska: summary of events and response of the Alaska Volcano Observatory. US Geol Surv Open-File Report 18:95–0271
- Neal CA, McGimsey RG, Doukas MP (1996) 1993 volcanic activity in Alaska: summary of events and response of the Alaska Volcano Observatory. US Geol Surv Open-File Report OF 21:96–0024
- Nye JF (1957) The distribution of stress and velocity in glaciers and ice-sheets. *Proc R Soc London Ser A* 239(1216):113–133
- Oddsson B, Gudmundsson MT, Edwards BR et al (2016) Subglacial lava propagation, ice melting and heat transfer during emplacement of an intermediate lava flow in the 2010 Eyjafjallajökull eruption. *Bull Volcanol*. <https://doi.org/10.1007/s00445-016-1041-4>
- Pierson TC, Janda RJ, Thouret JC, Borrero CA (1990) Perturbation and melting of snow and ice by the 13 November 1985 eruption of Nevado del Ruiz, Colombia, and consequent mobilization, flow and deposition of lahars. *J Volcanol Geoth Res* 41(1–4):17–66
- Pinkerton H, Wilson L (1994) Factors controlling the lengths of channel-fed lava flows. *Bull Volcanol* 56(2):108–120
- Raup BH, Racoviteanu A, Khalsa SS, Helm C, Armstrong R, Arnaud Y (2007) The GLIMS geospatial glacier database: a new tool for studying glacier change. *Global Planet Change* 56:101–110. <https://doi.org/10.1016/j.gloplacha.2006.07.018>
- RGI Consortium (2012) Randolph glacier inventory - a dataset of global glacier outlines, Version 1 [Data Set]. Boulder, Colorado USA. National Snow and Ice Data Center. <https://doi.org/10.7265/p9yk-6m11>. Accessed 8 Mar 2022
- Schaefer JR, Scott WE, Evans WC, Jorgenson J, McGimsey RG, Wang B (2008) The 2005 catastrophic acid crater lake drainage lahar and acidic aerosol formation at mount chiginagak volcano Alaska USA: field observations and preliminary water and vegetation chemistry results. *Geochem Geophys Geosyst*. <https://doi.org/10.1029/2007GC001900>
- Schilling S (2014) Laharz.py: GIS tools for automated mapping of lahar inundation hazard zones. US Geol Surv Open-File Report OF 78:2014–1073
- Self S, Sparks RSJ (1978) Characteristics of widespread pyroclastic deposits formed by the interaction of silicic magma and water. *Bull Volcanol* 41(3):196–212
- Sheridan MF, Wohletz KH (1983) Hydrovolcanism: basic considerations and review. *J Volcanol Geotherm Res* 17(1):1–29
- Smellie JL, Edwards BR (2016) *Glaciovolcanism on Earth and Mars: products, processes and paleoclimate implications*. Cambridge University Press, Cambridge
- Thouret JC, Gibert-Malengreau B, Vargas CA, Naranjo JL, Vandemeulebrouck J, Valla F, Funk M (2007) Volcano–glacier interactions on composite cones and lahar generation: nevado del Ruiz, Colombia, case study. *Ann Glaciol* 45:115–127
- U.S. Geological Survey (2018) 20191210, USGS Alaska 5 Meter AK IFSAR Eastern Aleutians Lot3 C358 2018 DTM n5600w15930P: US Geological Survey
- U.S. Geological Survey Scientific Investigations Report 2022–5075, p 32. <https://doi.org/10.3133/sir20225075>
- Valentine GA, Graettinger AH, Sonder I (2014) Explosion depths for phreatomagmatic eruptions. *Geophys Res Lett* 41(9):3045–3051. <https://doi.org/10.1002/2014GL060096>
- Van Eaton AR, Muirhead JD, Wilson CJ, Cimarelli C (2012) Growth of volcanic ash aggregates in the presence of liquid water and ice: an experimental approach. *Bull Volcanol* 74(9):1963–1984
- Walder JS, Costa JE (1996) Outburst floods from glacier-dammed lakes: the effect of mode of lake drainage on flood magnitude. *Earth Surf Proc Land* 21(8):701–723. [https://doi.org/10.1002/\(SICI\)1096-9837\(199608\)21:8<3c701::AID-ESP615%3e3.0.CO;2-2](https://doi.org/10.1002/(SICI)1096-9837(199608)21:8<3c701::AID-ESP615%3e3.0.CO;2-2)
- Waythomas CF (2014) Some geomorphic consequences of volcanic eruptions in Alaska. *Geomorphology* 246:123–145. <https://doi.org/10.1016/j.geomorph.2015.06.004>

- Waythomas CF, Walder JS, McGimsey RG, Neal CA (1996) A catastrophic flood caused by drainage of a caldera lake at aniakchak Volcano, Alaska, and implications for volcanic hazards assessment. *Geol Soc Am Bull* 108(7):861–871
- Waythomas CF, Miller TP, Wallace KL (2015) Surficial geologic map of mount veniaminof volcano, Alaska. *AGU Fall Meet Abstr* 2015:V33B-3091
- Waythomas CF (2021) Simultaneous effusive and explosive eruptions at Veniaminof Volcano, Alaska. *Volcanica* 4(2):295–307. <https://doi.org/10.30909/vol.04.02.295307>
- Welch BC, Dwyer K, Helgen M, Waythomas CF, Jacobel RW (2007) Geophysical survey of the intra-caldera icefield of Mt veniaminof, Alaska. *Ann Glaciol* 45:58–65
- Wilson L, Head JW (2007) Heat transfer in volcano–ice interactions on Earth. *Ann Glaciol* 45:83–86
- Wohletz KH (1986) Explosive magma-water interactions: thermodynamics, explosion mechanisms, and field studies. *Bull Volcanol* 48(5):245–264
- Wohletz K, Zimanowski B, Biittner R (2013) Magma–water interactions. In: Fagents SA, Gregg TKP, Lopes RMC (eds) *Modeling volcanic processes: the physics and mathematics of volcanism*. Cambridge University Press, New York, pp 230–257
- Waythomas CF, Dieterich HR, Tepp GM, Lopez TM, and Loewen MW (2022) The 2018 eruption of Mount Veniaminof, Alaska
- Yount ME, Miller TP, Emanuel RP, Wilson FH (1985) Eruption in an ice-filled caldera Mount Veniaminof Alaska Peninsula. In: Bartsch-Winkler S, Reed KM (eds) *The US Geological Survey in Alaska: accomplishments during 1983*. US Geol Surv Circ C 0945: 58–60

Publisher's Note Springer Nature remains neutral with regard to jurisdictional claims in published maps and institutional affiliations.

Authors and Affiliations

Christopher F. Waythomas¹  · Benjamin R. Edwards² · Thomas P. Miller¹ · Robert G. McGimsey¹

✉ Christopher F. Waythomas
cwaythomas@usgs.gov

¹ U.S. Geological Survey, Alaska Volcano Observatory, 4210 University Drive, Anchorage, Ak 99508, USA

² Department of Earth Sciences, Dickinson College, Carlisle, PA 17013, USA